2015

Pillars and Buttes: A Petrologic Comparison of Modern and Ancient Hydrocarbon Seep Rock

Erica C. Morelli
Oberlin College

OBERLIN COLLEGE

PILLARS AND BUTTES: A PETROLOGIC COMPARISON OF MODERN AND ANCIENT HYDROCARBON SEEP ROCK

HONORS THESIS

DEPARTMENT OF GEOLOGY

BY

ERICA MORELLI

KARLA PARSONS-HUBBARD, RESEARCH ADVISOR

OBERLIN, OHIO

MAY 2015

CONTENTS

ACKNOWLEDGEMENTS

PURPOSE

Literature on the formation of authigenic rock at cold seeps focuses on the role of microbes in creating geochemically favorable environment for the precipitation of carbonate and barite minerals. Less understood is the pathway that lithified microbial patches of seafloor sediment follow to become rock formations that are identified in strata dating back to the Silurian. In this study I will compare Holocene seep rock from the Gulf of Mexico to Cretaceous carbonates that have been identified as seep rock. Through the study of rock in its early stages of formation to rock that has likely undergone multiple phases of diagenesis I aim to establish a hypothetical sequence of formation of the Cretaceous seep rocks.

INTRODUCTION

Hydrocarbon seeps represent a burgeoning field of study for modern-day carbonate rock analyses. Though these types of petroleum seepage sites were relatively unknown for a long period of time, the past thirty years have led to a greater understanding of these environments as well as a better ability to recognize where seeps are occurring worldwide today (Table 1). In addition to modern day seeps, which are of particular interest to energy and oil companies, ancient seeps and their microbe-based ecosystems have been found in a variety of different geologic settings worldwide, with some dating from the Silurian and possibly as far back as the Cambrian and Proterozoic (Campbell, 2006). There exists a fairly vast diversity of seep types (Campbell et al., 2002) but similarities between modern seeps and ancient seeps can still be made based on commonly shared characteristics.

Hydrocarbon seeps are often grouped together with hydrothermal vent settings because both occur at continental margins or plate boundaries and exhibit effluence of chemical-rich fluids that allow for an association of microbial life and macrofaunal life to proliferate (Campbell, 2006). However, the two types of sites have significant differences in mode of effluence and conditions surrounding their respective environments. Hydrothermal vent settings are distinguished by the higher temperature of their effluence, which is heated by geothermal activity at active tectonic boundaries. The vent structures produced look similar to the structures seen at hydrocarbon (cold seep) sites, but differ in chemical composition and origin of formation. Cold/ hydrocarbon seeps typically form at passive continental margins and are the product of effluence of hydrocarbons released via tectonic activity. Current debate focuses on whether or not these hydrocarbons are sourced from the gas hydrate stability zone (400 to 1600 meters below the sediment-water interface at temperatures between 0 to 10 ^{o}C; Foucher et al., 2009).

Production of Authigenic Rock at Cold Seeps

The setting necessary for precipitation of carbonate rock in seep environments depends on an array of tectonic, sedimentary, biological, and chemical factors that are distinguishable at the microscopic scale. In the presence of methane and simple chain hydrocarbons, microbes and bacteria on the seafloor and within the sediment produce an extracellular polymeric matrix (EPS) that initiates the microbial and bacterial mat structures through trapping, binding, and precipitating sediment within the EPS. These mat structures are a crucial component of the hydrocarbon seep environment because they provide the substrate for further growth of additional microbes and macrofaunal species. Chemical and physical factors at seeps create gradients and microenvironments that allow for the growth of different species of microbes and bacteria. Beneath the mat and within the sediment, a zone of reduction is established through the addition of nitrate, ferric iron, tetravalent manganese, and sulfate into the system that allow anoxic oxidation of organic carbon (Stolz, 2000). At this zone, organic matter is oxidized and sulfate is reduced to produce bicarbonate ions through the reaction:

$$2CH_2O + SO_4^{2-} < > H_2S + 2HCO_3^- \quad (1.1).$$
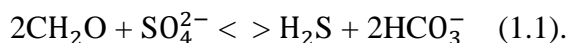
In the presence of available calcium ions, the carbonic acid then reacts to precipitate carbonate rock as in reaction:

$$Ca^{2+} + 2HCO_3^- < > CaCO_3 + CO_2 + H_2O \quad (1.2).$$

An alternate pathway can additionally lead to the production of bicarbonate (1.2), if methane is the hydrocarbon present, as seen in reaction:

$$CH_4 + SO_4^{2-} < > HS^- + HCO_3^- + H_2O \quad (1.3).$$
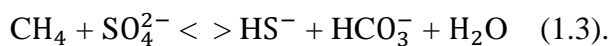
Seafloor microbial mats can become lithified and preserved in the rock record as evidenced by a number of fabric types that have been observed at thin-section scale. The lithification process includes a degree of ammonification, denitrification, sulfate reduction, and anaerobic sulfide oxidation, which lead to the precipitation of micritic fabrics. Lithification traps micritic sediments that have accumulated within pore spaces via reactions 1.1 through 1.3, which becomes substrate for further microbial growth, thus creating a positive feedback loop of microbial mat production. It is commonly observed that the primary fabric type is a laminated stromatolitic texture of calcified spar-encrusting microbes and the primary to secondary fabric type is a clotted thrombolitic texture (Riding, 2000; Figure 1). The textures in this study have mainly been classified as clotted thrombolitic.

Underneath microbial mats, the changes in pore water chemistry lead to calcium carbonate ($CaCO_3$) deposition. Bacteria and archaea catalyze the precipitation reaction (1.3) via anaerobic oxidation of methane (AOM), which leads to the formation of seafloor authigenic carbonates (Bailey et al., 2009). The Bailey et al. study indicates that chemoautotrophic microbes occupy the interfaces between oxidized and reduced chemical species, which leads to the formation of microbial reefs. When reefs form with methane seeps, sulfate, and anoxic bottom waters, they can be partially lithified with calcium carbonate and begin forming in subsurface environments. This may cause macroscopic precipitation of a calcareous core that leads to growth in the water column as visible columnar or chimney-like structures (Treude et al., 2005).

BACKGROUND OF SITES

Gulf of Mexico

The continental shelf and slope of the Gulf of Mexico represents one type of methane

seep environment. The formation of carbonate in surface sediments of the Gulf of Mexico

(GOM) shelf and slope depends upon the migration of hydrocarbons and some sites exhibit

precipitation of barite whose origin is unclear. Although the origin of barite is unknown, it is

thought to precipitate from barium super-saturated formation waters that may originate from

biogenic input through the water column (Aharon, 2003). In the GOM, intense periods of

sedimentation and movement of subsurface salt layers resulted in numerous configurations of

domes and basins on the continental slope (Roberts and Aharon, 1994; Figure 2). During Late

Jurassic time, the Louann Salt Formation in the Gulf area acted as a seal rock and trapped

hydrocarbons beneath it. Migration of the salt caused faults to develop in overlying strata.

Throughout time, movement of the salt layers distorted the salt into irregular diapirs causing a

fault network to develop through the rising of these salt diapirs. The overlying rock allowed the

seepage of hydrocarbons from below the Louann salt up to the sediment-water interface through

these conduits (Aharon, 1994; Figure 3).

Chemosynthetic bacteria fix hydrocarbons that seep through the seafloor, which leads to

the precipitation of carbonate rock. The interplay of the carbonates formed and the associated

hydrocarbon emissions are defined as "chemoherms" (Aharon, 1994). Chemolithotroph

communities of microbes that undergo oxidation of reduced sulfur compounds are associated

with chemoherms and are supported by habitats that experience oxic to anoxic transitions. The

role of thiotrophs (sulfur-oxidizing bacteria) and methanogens and methanotrophs (methane-

oxidizing bacteria) are indispensable in this process as they alter the chemistry of the carbon,

sulfur and nitrogen dissolved in seep pore fluids, which allows the super-saturation of carbon dioxide (reactions 1.1 - 1.3). Carbonate rock is precipitated if this process is coupled with highly alkaline water and a high Dissolved Organic Carbon (DIC) content (Aharon, 2003). Carbon dioxide can come from several different sources including: methane oxidation at the sediment-water interface; aerobic oxidation of organic matter in the water column; and aerobic fermentation/ sulfate reduction (Aharon, 2003). In a recent article by Bian et al. (2013), precipitated carbonate is found to form in three large-scale structures, based on their method of formation. All structures were found to include seawater in the precipitation process and mostly precipitated high-Mg calcite or aragonite (Bian et al., 2013). The young carbonate rocks used in this study on the Northern Gulf of Mexico are also high-Mg calcite with some aragonite constituents and can be classified using this method.

Tepee Buttes

Hydrocarbon seep environments are also found preserved in Cretaceous rock from the Tepee Buttes Formation in Colorado. While these rocks no longer exhibit carbon fixation to create carbonate rock, they are remnants of microbial processes that likely occurred during the Late Cretaceous in the Western Interior Seaway (Figure 4). Situated within the Upper Cretaceous Pierre Black Shale, these mound-like structures are noted to occur in distinct lines parallel with the Laramide Orogenic Faults (Shapiro and Fricke, 2002; Figure 5). It is thought that these buttes formed at spring-like submarine seep sites with diverse and abundant marine communities, similar to the diversity of organisms associated with modern day analogues (Kauffman et al., 1996). The influx of hydrocarbon-rich water from the surrounding Pierre Shale and Niobrara Formations and microbial activity led to precipitation of carbonate rock (see reactions 1.1 to 1.3)

subsequent weathering formed the present-day carbonate mounds (Figure 6). Generally, the

mounds formed intermittently at 30 to 100 meter water depths during the Late Cretaceous for

1.25 million years (Kaufman, 1984).

Shapiro (2000) classifies these rocks as thrombolites, or more descriptively, as

thrombolitic microbialites. The thrombolite distinction comes from the existence of a host of

macro and meso structures that are present in nearly all the Tepee Buttes throughout the former

Western Interior Seaway. It is currently believed that thrombolites represent microbialites that

are composed of a clotted mesostructure in which mesoclots such as peloids and calcite to

aragonite cement are the mesostructural components (Shapiro, 2000). These thrombolitic

structures are widely accepted to be ancient analogues of modern hydrocarbon seep structures,

such as those present in the Gulf of Mexico rocks. It is proposed that symbiotic chemosynthetic

bacteria are associated with carbonate precipitation because of their resemblance to modern seep

carbonates and from possible evidence seen in the occurrence of sulfides, silica replacements,

and microcrystalline calcite in molds found in rock samples of the Tepee Buttes (Shapiro &

Fricke, 2002). Additionally, the authigenic carbonate, as well as some of the barium sulfate

minerals observed in these seep settings, may originate from the microbially mediated process of

anaerobic oxidation of methane (Campbell, 2006).

The processes that produce the ancient seep rock are complex due to a long period of

diagenesis. Campbell, et al. (2002), suggest that during early diagenesis of ancient seep rocks

from the Mesozoic convergent margin of California, a period of corrosion created vugs and

residual micrite regions that later engulfed younger cement, followed by crystallization of yellow

calcite, organic matter, pyrite and then botryoidal cement. The later stage of diagenesis of these

rocks involves the precipitation of yellow calcite, which is then sometimes coated with

framboidal pyrite. Vug and pore-filling sparry calcite are also indicators of later burial diagenesis. Once these transformations are complete and nearly all pore spaces are filled, the carbonates behave as a closed diagenetic system (Campbell et al., 2002).

Tepee Buttes rocks contain many similar components to the Mesozoic rocks studied by Campbell (2002). In 2006, Anderson also ranked Tepee Buttes rock at thin section scale based on the Folk Classification System for carbonate rocks and split the fabric types into: pelmicrite, pelsparite, micrite, sparite, and intrapelsparite (Table 2). Anderson further split the carbonate textures into growth stages: yellow calcite phase first, followed by the growth of botryoidal calcite, and finally by the growth of sparry, void-filling calcite (Anderson, 2006).

I propose that the Gulf of Mexico carbonates are good modern representatives of seep rock formation at its earliest stages. Thus, I will compare Cretaceous carbonates that have been identified as cold seep carbonates, to these modern rocks to build a history of formation and diagenesis in cold seeps. This study hopes to expand upon Anderson's classification of Cretaceous seep carbonates and call to question her proposed stratigraphic method of formation in the Tepee Buttes rocks. My aim is to use a comparison of the Tepee Buttes to the Gulf of Mexico Pillar Rock to show an alternative method of conduit formation of the Buttes. Similarities between the two might bring to light a standard process of formation of hydrocarbon seep rocks that can be seen across varying environments and could be used to recognize and interpret fossil seep systems.

SAMPLE AREAS

Gulf of Mexico Samples

The Gulf of Mexico seeps surveyed in this study are comprised of several different sites

throughout the continental slope, with a specific focus on the OCSG Pillar Rock site. The OCSG

Pillar Rock is located in the Outer Continental Shelf offshore from Galveston, TX (~150km

SSE). This rock exists as a large pillar with its visible base at roughly 190 meters below the

surface of the water. This chimney-like structure is about 4.5 meters tall and has no obvious

central conduit, which may indicate that it has diffuse conduit holes existing throughout the

entirety of the structure (Figure 7). Life is ubiquitous at this site in comparison with the barren

muddy seafloor surrounding the pillar. Fish and crab are found close by and there is an

abundance of sponges associated directly with the structure. Samples from this site were

collected on several different days with the initial discovery made in the summer of 2006 by the

Shelf and Slope Experimental Taphonomy Initiation (SSETI) research group. All samples exhibit

a highly porous texture with abundant boring and conduit holes as well as a variety of different

macro (clams, sponges, etc.) and micro (bryozoans, foraminifera, etc.) faunal associations. The

rocks are generally grayish in color but exhibit some degree of red-brown discoloration via

oxidation. This indicates that some amount of iron must be present in the formation or the rocks

were exposed to oxygenated conditions at some point in the past. Samples from the Pillar Rock

site were labeled by date sampled or location of storage. Samples analyzed included

OCSG83106, OCSG90106, and OCSG Bucket #3 (OCSGB3).

Other sites from which samples were collected, but were not extensively analyzed in this

study, are Green Canyon site 272 (GC272) and Garden Banks site 425 (GB425). Green Canyon

represents a similar carbonate rock site associated with hydrocarbon seepage but with a different

pattern of precipitation that appears predominantly muddier and less bored by fauna. Garden

Banks represents a different type of seep site entirely: the primary precipitated constituent is

barite rather than carbonate and the site has an entirely different set of faunal associations than

the Pillar Rock site. The GB425 rock samples exhibit banding textures on the hand sample scale

that show alternating layers of bluish barite rock and layers of white barite rock. These generally

appear to occur semi-concentrically around what appears to be a main conduit space. Fu et al.,

noted similar banding textures at barite sites in the Gulf of Mexico (1994).

Tepee Buttes Samples

   Parsons-Hubbard, Shapiro, and students collected Tepee Buttes samples from several

different locations during field collections in 2005 as part of an NSF-funded project of the Tepee

Buttes. Of the samples collected, I initially determined that the Buttes could fit into one of two

categories: vuggy, heavily cemented rock with abundant peloids and rock with an abundance of

lucinid bivalve remains. I chose to focus on Butte 326.5 (007) and Butte 710 (014) in this study

because I felt they were rough representations of these two categories; Butte 326.5 being mostly

of the vuggy rock and 710 mostly of the bivalve rock (Figure 8). The 300 series of buttes are

found in the Boone Road cut location (Figure 9) and the low to high 700 series buttes are found

in the North Ranch location (Figure 10). The Boone Road and North Ranch locations reflect

different geographical locations in Colorado with the Boone Road buttes being closer to Boone,

CO in Pueblo County and the South to North Ranch buttes being located closer to Colorado

Springs, CO.

METHODS

I. Petrographic Procedures

Point Counting and Transect Analysis

Point counting was used to make an initial classification of rock types and to determine the rock type of the Gulf of Mexico samples. This determination was used to place the samples within the Folk Classification scheme (Folk, 1962) for a better comparison with the Tepee Buttes. Pictures of thin sections were taken using a Leica microscope with a LAS EZ camera. Photomicrographs of each thin section were taken at 40x magnification and processed in Adobe Illustrator on which a 10x10 grid was superimposed. At the meeting of each crosshair, bioclasts, micrite, or cement was recorded for a tentative determination of general rock composition. For both the Pillar Rock and the Tepee Buttes samples, 50 points were counted for each image. Specific numbers of spots (per photomicrograph) for sample thin section slides can be seen in Table 3.

Areal Determinations of Fabric Types

Using the National Institute of Health's freely available ImageJ software, thin section photomicrographs (4x magnification) from the Gulf of Mexico and Tepee Buttes samples were analyzed to determine the areal percentage of different fabric and cement types present in each sample (samples used shown in Table 3).

Using a classification scheme created for this project which is based on determinations of fabric type variance from the Folk Classification System, constituents of these samples were grouped into seven major categories: 1) Sparry calcite cement, 2) Allochems, 3) Hole and/or pore space, 4) Micritic peloidal matrix, 5) Botryoidal cement, 6) Yellow calcite, and 7) Muddy

accumulated sediment. Point counting was used initially as a first approximation of what was in the Pillar Rock versus the Tepee Buttes and aided in creating these categories. In this study, allochem refers to a clump of peloidal and micritic material that may have origins during the original lithification on the seafloor but also includes other constituents that are not original to the matrix of the rock. In ImageJ, thin section and acetate peel photomicrographs were traced using the freehand trace tool to create a polygon surrounding a particular type of cement or fabric. Pixel area of that polygon was measured and recorded in units of pixels squared. Total area of each type of cement/fabric was calculated against the pixel area of the entire image to show the percentage of each type present in a given photomicrograph. The areal percentage method, instead of point counting, was used for final analysis of constituents because it proved to be more accurate amongst samples.

Acetate Peels

In order to analyze the textural properties of the rocks sampled, acetate peels were made from two of the Tepee Buttes hand samples and one of the Pillar Rock hand samples (Table 3). This method was used to reveal a greater level of textural detail than seen with the thickness of the standard thin section. Samples were cut in half and polished with grit to achieve an even surface. The smoothed surface was washed and prepped for the peeling process. Acetone was poured onto the smooth surface and a piece of acetate paper was applied and smoothed out to free the surface of bubbles and aid in adhesion. The acetone-acetate treated rocks sat for roughly 15 minutes, after which the peel was ripped off of the rock, causing a thin layer of rock to adhere to the acetate sheet. The standard thickness of these sheets (< 20 microns) is much thinner than the standard thin section used in this project.

II. Techniques for Determining Terrigenous Content

Staining

Both Tepee Buttes and Gulf of Mexico samples were stained to better distinguish between carbonate and terrigenous material and between different types of calcium carbonate in thin section. Using the methods elucidated on the University of Cambridge Geology Department website, a solution of 300ml 0.5% HCl was mixed with 0.6g Alizarin red S (and filtered) while a solution of 200ml 0.5% HCl was mixed with 4g potassium ferricyanide. After the Alizarin red solution was fully filtered, the two solutions were mixed together in a 600ml beaker. Thin sections were held with tweezers for better precision and dipped halfway in the staining solution for 45 seconds. Half-and-half dipping was done in order to create a comparison point of dyed slide to non-dyed slide. After staining, the entire section was rinsed with deionized water and stood against a beaker to dry.

Digestion

An acid digestion was performed to measure the percentage of terrigenous material present in Pillar Rock and Tepee Buttes samples. Small pieces weighing roughly 25 to 150 grams each were washed and dried in an oven for 4-6 hours. A 10% HCl acid solution was prepared and a sample of cleaned and dried rock was weighed, recorded, and placed in the acid for 12-36 hours or until the digestion process was complete. After digestion, each individual sample was filtered for an additional 12-24 hours to collect the leftover terrigenous material on a piece of filter paper, after which the filter paper sample was placed back in the oven to dry for 4-6 hours.

With the drying complete, the sample was weighed, recorded, and calculated for percentage of terrigenous material.

To confirm the accuracy of the terrigenous mass percentage calculation for each sample, point-counting methods of stained samples were employed to compare the number of points of terrigenous constituents to the number of carbonate constituents. Using the staining method, thin sections of Pillar Rock (Bucket #3 and OCSG83106; Table 3) were stained and analyzed using a Petrographic microscope. Pictures were taken of the thin sections using a Leica Microscope with a LAS EZ camera at 40x magnification. Pink textures denoted areas of fine-grained carbonate matrix and unstained matrix denoted terrigenous material. Using Coral Point Counting software (CPCe version 4.1), the photos were processed to overlay a randomization of 30 crosshair points over the entire picture. Points were counted as carbonate or terrigenous based on what the crosshairs intersected; any crosshairs that intersected holes or cracks fell into a third category of 'other'. After points were collected, totals and percentages were calculated for the pictures and compared with the percentages calculated from the acid digestion process.

Scanning Electron Microscopy

Two main methods of microscopy were employed for the analysis of textural and chemical composition of these rocks. Using JEOL-SEM and Oxford Electron Dispersive Spectroscopy (EDS) software in the Oberlin College Geology Department, thin sections from the Tepee Buttes as well as Pillar Rock (Gulf of Mexico) were carbon coated and analyzed using both Scanning Electron Imaging (SEI) and Back-Scatter Electron (BSE) imaging. SEI imaging allows for analysis of crystal microstructures in thin section and BSE detection can acquire chemical data for those crystals and other areas of interest in the samples. BSE was mainly used

to determine the relative amounts of smaller constituent minerals such as barite and pyrite, which are present in the Tepee Buttes and Pillar Rock (samples used in Table 3). Stub samples were made to photograph crystal structures of Gulf of Mexico samples (OCSG83106 and GB425) and locate differences in cement types based on differences in topographic expression of crystal structure. Certain geometric forms visible at high magnification can reveal differences in fabric types that otherwise appear the same in petrographic methods (e.g. barite rosettes, pyrite framboids, etc).

III. Techniques Used to Identify Later Diagenetic Changes

Cathodoluminescence Petrography

Cathodoluminescence Petrography (CL) can provide visual cues to understanding the diagenetic relationships between grains, matrix, cements, porosity evolution, and replacements that occur in carbonate rocks (Hiatt and Pufahl, 2014). CL Petrography was conducted on a Relion ELM-3R Luminoscope with a Nikon Coolpix camera attachment at Chico State University courtesy of Professor Russell Shapiro. Photomicrographs of an area of interest were taken to document the site for comparison with possible luminescence. Voltage was held at roughly 10 to 12 kV, the current was held at roughly 0.037 DCmA, and the chamber vacuum was held between 30 and 60 millitorr. Final images showing luminescence were taken of each area and saved to an external hard-drive for later processing.

Isotope Geochemistry

Stable isotopes of carbon can reveal bacterial activity present in the formation of carbonate and with the addition of oxygen isotopes can track diagenetic fluids between individual petrofabrics (Anderson, 2006). In addition, decreasing values of $\delta^{18}O$ can indicate fluid-rock alterations (during metamorphosis and diagenesis) but diagenetic modifications are not as apparent from the $\delta^{13}C$ values.

Stable isotope analyses of seventeen samples amongst Pillar Rock and Tepee Buttes hand samples (Table 3) were conducted at the University of Alabama Geological Research Facility with a DeltaPlus mass spectrometer with gas dispenser. Under the direction of Dr. Paul Aharon and Dr. Joe Lambert, powdered samples from selected textural phases chosen via thin section were collected using a drill machine in the Alabama Stable Isotope Lab (ASIL). Most locations for Pillar Rock seemed to exhibit a mottled or slightly alternating blue and white fabric pattern. Most samples were drilled in the center of mottled white and blue blocks with the exception of a sample that was collected along the rim of a conduit hole and a sample collected at the rim of a hole created by a tubeworm. Powdered samples between 60 and 105 micrograms were weighed and collected in small glass vials. Samples were recorded and labeled by sample type and weight using Isodat 2.0 software. All samples were loaded and placed amongst various standards with similar weight amounts (NBS-19) and underwent a CO_2 gas exchange and a Helium gas exchange before being injected with an acid to convert the powder to a gaseous phase for analysis. After completion of these steps, stable isotopes of carbon and oxygen were collected for each vial and subsequently compared to and corrected against the standards. The universal standard of Vienna Pee Dee Belemnite (VPBD) was used for comparison of isotopes.

RESULTS

The Gulf of Mexico samples are generally classified as biomicrites while the Tepee Buttes rocks are classified as pelbiosparites due to the large amount of calcite and aragonite cementation as well as the abundance of peloids (Folk, 1962; Table 2). This initial classification is based on observations of hand samples and the work of Anderson (2006) and was used to help direct further analysis from methods used in this study.

Pillar Rock

I. Fabric Types

Point-counting methods reveals that the Pillar Rock samples contain 12% bioclastic material while over two-thirds of the rock qualifies as lime-mud matrix, placing the Pillar samples under the Sparse Biomicrite category (Table 2). Collection of data using the areal percentage method revealed that the Pillar Rock is primarily composed of micritic peloidal matrix at roughly 80% of the total sample data collected (Table 4). The next largest constituent is void or pore space at ~12%, followed by botryoidal cement (~6%) and muddy accumulated cement (~3%). In general, the Pillar Rock does not exhibit the same diversity of fabric and cement types as the Tepee Buttes samples.

Digestion of several samples (Table 3) from the Gulf of Mexico OCSG Pillar Rock reveals that the carbonate generally consists of roughly 16 ± 7% terrigenous material and 85 ±

7% carbonate material. Point counting also confirms the values 13 ± 3% terrigenous material and 87 ± 3% carbonate material. Results are shown in Table 5.

II. Relationships Between Fabric Types

In hand sample, the Pillar Rock exhibits a homogenous texture within discretely defined blocks, which are categorized as fundamental building units of the conical pillar structure (Figure 11). In thin section, these blocks are generally indistinguishable, but heterogeneous zones are found in several areas of thin section photomicrographs, that are indicative of the block units. Small peloids (~ 0.20 - 0.50 microns) appear to be embedded in the micritic matrix and are generally of a larger grain size than that of the matrix. Micrite is defined as the general fabric of the blocks and can include the small peloids, dendritic pyrite textures, siliciclastic bits (~0.2 – 0.5mm; Figure 12), and shell fragments of foraminifera. Some blocks contain an abundance of shell fragments, peloids and dendrites within the micrite and others have siliciclastic inclusions in the micrite (Figure 11). Blocks can be distinguished in thin section by the differences in these constituents. Another distinct texture is an alternating blue and white mottled texture (Figure 13), visible in both thin section and hand sample; of this texture, white appears to be the overwhelming constituent in hand sample. Blue appears reddish brown in thin section. Some of these areas are more porous than the typical micritic peloidal matrix.

Small pore spaces and zones between different blocks have botryoidal calcite growth (Figure 14). Some blocks have boring holes that are defined by sharp boundaries while others were cut by conduit holes that are defined by less distinct boundaries with a stained rim surrounding the entire hole (Figure 15). In general, blocks are cross cut by a diffuse array of conduits; there is no apparent central conduit around which the blocks accrete. There is an even

split between unfilled holes (either boring or conduit), muddy accumulated sediment filled holes, and partially cemented holes.

III. Isotopic Signatures of Fabric Types

Isotopic analyses of the Pillar Rock reveal some variations in carbon and oxygen stable isotope values (Tables 6 & 7). Carbon ($\delta^{13}C$) values range between -33.6 and -40.4 ‰ VPDB and oxygen ($\delta^{18}O$) values between 1.9 and 2.2 ‰ VPDB.

Generally, the stable isotope signatures for the Pillar Rock samples did not vary significantly, especially in the case of the oxygen stable isotope values. It should be noted that there are few differences between the hand sample and thin section fabric types for each sample location from which powder sampling was conducted. In general, the sample values hovered between the -36 and -40 ‰ range with the exception of two locations, which had significantly lower values (-33 and -34 ‰). When these sections were compared with the thin section and hand sample locations that were initially sampled, these values correlate with locations of higher porosity and increased cementation. The other locations (with -36 to -40 ‰ $\delta^{13}C$ values) correlate with areas of much denser micrite. Locations on samples that have a denser micritic composition exhibit a higher degree of pyritic framboids. This does not hold true for the more porous and highly cemented locations, which have a higher degree of botryoidal growths apparent in thin section, but do not exhibit the same density of pyritic framboids as the other locations.

IV. Other Features

Secondary Electron Imaging (SEI) microscopy and back-scatter electron detection (BSE) for the Gulf of Mexico Rocks revealed a significant weight percentage of iron inclusions with the highest hovering around ~45% for individual spot analyses (Figure 16). Some samples had much lower iron signatures but this was likely from the location of the spot surveyed during BSE analysis. Locations that were closer to the rims of conduits and boundaries tended to have higher iron signatures due to the abundance of pyrite framboids (Figure 17) in these areas.

Tepee Buttes

I. Fabric Types

Based on areal percentages as well as the work of Anderson (2006) and Shapiro (2002), Tepee Buttes samples were tentatively classified as pelbiosparites due to the high percentage (~23%) of sparry calcite cement as well as high percentage of allochems made of peloids and peloidal matrix (~27% and ~28% respectively). With well over half of the rock consisting of some sort of spar or peloidal constituent, these samples align with other classifications of the Tepee Buttes (Anderson, 2006). Tepee Buttes samples exhibit a fairly even split between micritic peloidal matrix (~28%), allochems (~29%), and sparry calcite cement (~23%) as the dominant constituents (Table 4). Other constituents represented in these samples include botryoidal cement (~ 14%), followed by yellow calcite (~6%). Void/pore space is present, but only in a negligible quantity (~0.2%). Generally, the fabric types seen in the Tepee Buttes represented a similar but more diverse array than those seen in the Pillar Rock.

II. Relationships Between Fabric Types

        In the Tepee Buttes, the micritic peloidal matrix contains peloids smaller than ~0.50 microns, very few shell and foraminifera fragments, and has small inclusions of siliciclastics and dendritic or framboidal pyrite (Figure 18). The boundaries between this fabric type, allochems, and sparry calcite can be poorly-defined and as in Figure 19, can morph into space containing an abundance of peloids larger than ~0.50 microns. However, allochems are a distinct fabric type from the sparry calcite and from the micritic peloidal matrix. There is a range of material that can be included in an allochem, but generally they encompass areas that contain bits of relict fabric types and/or peloids that are surrounded by yellow calcite growth and held together with a different stage of botryoidal calcite growth (Figure 19). The peloids included in allochems tend to be larger and have more than one contact per grain. Some allochems contain pieces of the micritic peloidal matrix that are surrounded by isopachous rims of yellow calcite (Figure 20). The larger peloids that are not part of an allochem tend to have less than one contact per grain and thus constitute a self-supported detrital framework. The peloids in these areas are not surrounded by yellow calcite but appear to be further cemented by botryoidal calcite (Figure 21).

        Void spaces are apparent in hand sample, primarily in Butte 326.5, and are randomly dispersed throughout the thin sections. Most voids have fuzzy boundaries and contain sparry calcite. The boundary between allochems and the sparry calcite void-fills is especially evident in areas where there are thick yellow calcite growths (Figure 22). A different occurrence of sparry calcite is seen in the remains of bivalve shell fragments. This cement can either be contained within the confines of the shell fragment or can extend to the inner part of the shell and around

allochems (Figure 23). Bivalve shell fragments cross cut some peloids and allochems in several areas but also have peloids directionally oriented within them in other areas (Figure 24).

Other textures that should be noted are roughly concentric-like gray rings within many areas of the micritic peloidal matrix (Figure 25). Significant siliciclastic material was also noted in the Buttes samples with grain sizes ranging from ~0.01 to 0.2 mm in largest dimension (Figure 12).

III. Cathodoluminescence of Fabric Types

CL petrography reveals that Pillar Rock samples did not luminesce, while many sections of the Tepee Buttes rocks luminesced dark red. Differences in luminescence of sparry calcite were noted between vug/pore spaces, veins, and bivalve segments (Figure 26). In general, peloidal micritic matrix did not luminescence while botryoidal cement exhibited weak to no luminescence.

IV. Isotopic Signatures of Fabric Types

Two samples from Tepee Buttes (Buttes 326.5 and 710; Table 3) were compared with the Pillar Rock. All samples reveal similar ranges of carbon isotopes (-12.5 to -37.1 ‰ VPDB) but the Pillar Rock exhibited much heavier oxygen values, which ranged from -2.9 to -12.2 ‰ VPDB.

Tepee Buttes samples exhibit a greater variation in carbon stable isotope signatures than the Pillar Rock. Three fabric types were sampled: yellow calcite, sparry calcite, and a mix of allochems and micritic peloidal matrix that were grouped together for the purposes of analysis due to the uncertainty introduced in connecting thin section photomicrographs to the sites within

each sample (Table 8). Sparry calcite locations seemed to exhibit a higher carbon isotope signature, with values of -12.5, -22.5, -23.1, and -23.9 ‰. Yellow calcite was often partially mixed with allochems and/or matrix, which complicated the connections to certain $\delta^{13}C$ values. In general, the yellow calcite and allochem/matrix values were roughly the same with values falling between -30.0 and -32.0 ‰ $\delta^{13}C$. One outlier was noted with a value of -37.1 ‰ and a higher value of $\delta^{18}O$ at -5.9 ‰. Oxygen stable isotope values generally fell between -10 and -12 ‰, but the outlier sample that had a higher value of $\delta^{13}C$ also had a much higher value of $\delta^{18}O$ at -2.9 ‰ (Table 8).

V. Other Features

BSE detection of the Tepee Buttes rocks showed a high iron content ranging between ~20 to ~60 wt% (Figure 27). Tepee Buttes rocks additionally had areas with significant signatures for barium and some strontium. At the locations where barium occurred, weight percentages tended to range between ~40 and ~57 and are associated with strong sulfur signatures, indicating that the mineral being sampled was likely barite (Figure 28).

Garden Banks

Though the main precipitates at seep sites in the Gulf and elsewhere are of carbonate rock, other types have been discovered. The most anomalous of these are the barite seep environments observed in rock samples from this study as well as observed and described extensively by Paul Aharon in a study of Gulf seep sites from 2003 (Aharon, 2003). One of the

sites surveyed in this study, Garden Banks (GB425), exhibits barite chimneys, confirmed with SEM analyses of epoxy-impregnated thin sections and stub samples of the rock; on average, thin sections contained ~51 wt% barium (Ba), ~15 wt% sulfur (S), and ~3 wt% strontium (Sr; Figure 29). Other elements, such as calcium, appeared in several of the locations analyzed but did not represent a significant weight percentage. Characteristic rosette crystal structure for barite growth was also observed in a sample from Garden Banks site 425 (Figure 30).

DISCUSSION

Micro to Mesostructural Formation

Hydrocarbon seep environments can be identified by a number of different factors, including shape of the rock structure, visible effluence of hydrocarbons, and abundances of macro-fauna in areas of the seafloor that are otherwise desolate. These characteristics were all noted for the Pillar Rock site, which exhibits a typical conical to pillar-like rock formation (Figure 7). Video footage of the Pillar Rock site taken by the SSETI team members Karla Parsons-Hubbard, Rick Krause, and Kathryn Ashton-Alcox in 2006, showed small locations of what was potentially active seepage of hydrocarbons. Video footage and photographs taken on site also show associations of several different types of macro-fauna, including several species of clams and sponges. Larger fish and crabs are commonly found around these sites, likely secondary beneficiaries of the seep ecosystem.

Evidence of microbial activity is noted in video footage of the surrounding Pillar Rock area and other sites nearby the Pillar Rock that exhibit typical white microbial mats on the

27

seafloor that have been noted in other studies of the Gulf of Mexico (Roberts & Aharon, 1994). The alternating nature of the blue and white lamination textures in hand samples of the Pillar Rock are also indicative of a microbial mat formation mechanism: mats tend to preferentially grow towards the surface as sediment accumulates on top of them over time (Treude et al., 2007; Figure 31). While these attributes are easily noted for the modern-day Pillar Rock, they are hard to distinguish and sometimes impossible to note in the Cretaceous Tepee Buttes samples. Despite the great span of time between the creation of the Pillar Rock and the Tepee Buttes, the evidence of microbial activity indicates that both locations represent examples of hydrocarbon seeps.

Both the Pillar Rock and the Tepee Buttes sites examined in this study exhibit micrite cement as the predominant fabric type, indicating that these sites at least began with the same fundamental building block. The main difference between the modern and ancient sites is the presence of allochems in the Tepee Buttes sites. The allochems are representative of a different stage of fabric formation that likely happened post-micrite formation and after subsequent diagenetic events that could have created pore spaces into which the allochems accreted. Allochems host peloids with isopachous rims, which are evidence for the Tepee Buttes structures being exposed in marine water for sometime during their diagenetic history. The allochems were likely later cemented in place through the introduction of sparry calcite into these voids possibly after the Western Interior Seaway drained and the rock formations were buried in sediment (or vice versa). Additionally, the barite signature present throughout Butte thin section samples can be explained through the continuous input of marine waters over time throughout the Western Interior Seaway, because barium is a relatively common mineral at depth in ocean water.

Barium was also observed in an entirely different type of seep environment in the Gulf of Mexico. A study by Aharon (2003) revealed that samples of barite ($BaSO_4$) that precipitate from

Garden Banks and the Auger Basin are from mudflow environments that have depositional lobes with distinct boundaries. The mud erupting at these sites showed an anomalous enrichment in Sr, Ca, and Ra. The current hypothesis for the formation of barite from these constituent waters is the connate model, which suggests that the advection in deep-seated, methane-rich formation waters along fault conduits brings in fluids rich in Ba, Ra, Sr, Cl, and Ca but deficient in sulfate. When these fluids come in contact with the sulfate-rich seawater, they become supersaturated with barium and sulfate/ide and lead to the precipitation of barite chimneys (Aharon, 2003). No barite was found in the Pillar Rock samples.

In the Pillar Rock, SEM and petrographic analyses reveal significant groupings of pyritic compounds with a typical framboidal growth formation (Figure 17). These groupings of iron-sulfides are hypothesized to be corrosion products of sulfate-reducing bacteria (SRB; Enning and Garelfs, 2014) and thus, direct evidence of SRB. SRB live within the sediment and fix the hydrocarbons to preferentially form the carbonate mud-matrix that is extremely abundant in the Pillar Rock samples, taking up roughly ~80% of the total rock type from the samples surveyed. They leave behind elemental sulfur, which can then react with available ions to create the framboid or dendrite structures seen in thin section.

Similar to the Pillar Rock, BSE analysis of the Tepee Buttes rocks show a significant iron signature and petrographic methods reveal a similar abundance of pyritic framboidal structures, potential evidence of sulfate-reducing bacteria (SRB). The general appearance of these framboidal structures is almost identical to the Pillar Rock and framboids are found in the micritic peloidal matrix of this site and the Tepee Buttes sites. Due to the older age of the Tepee Buttes rocks, direct evidence of microbial mats was not found. Additionally, their significant diagenetic overprinting over geologic time, as noted by the much higher abundance of cement

fabric types may have contributed to the lack of true microbial signatures. However, further evidence of microbial activity, through petrographic surveys of several of the Tepee Buttes thin sections, is seen by the characteristic patterns of roughly concentric growth rings of a more grayish color as compared with the surrounding micritic peloidal matrix (Figure 25). These concentric gray rings are evidence of microbial activity because they represent denser, clotted (thrombolitic) areas of the precipitated rock that formed through microbial trapping of sediment and subsequent lithification (Riding, 2000). Thus, I hypothesize that the micritic matrix of the Tepee Buttes rocks had a similar mode of formation to the Pillar Rock with significant sulfate-reducing microbe activity. It is likely that several different types of microbes existed in the Tepee Buttes (and in the Pillar Rock) that were active in forming the micritic peloidal matrix. For this reason, I establish that the micritic peloidal matrix - represented by the grayish-bluish fabric type in the modern Gulf seep rocks correlates with the tannish fabric type in the Tepee Buttes samples. Therefore, the micritic peloidal matrix is the fundamental building block of hydrocarbon seep sites and can be identified across many different locations and even across geologic time.

Seep Rock Formation

Comparisons between the Pillar Rock and the Tepee Buttes lead to an emerging picture of the mode of formation of authigenic carbonate at hydrocarbon seeps. The first stage is the series of chemical reactions (reaction 1.1-1.3) via sulfate reduction and/or anaerobic methane oxidation (from methane-oxidizing Archaea) that lead to an alkaline microenvironment with an abundance of calcium ions that cause the precipitation of the micritic peloidal matrix. This likely happens somewhere between the sulfate-methane interface (SMI) and the sediment-water interface (SWI) depending on the sample and the amount of oxygen available to the microbes.

30

The sulfate-methane interface occurs at around 60-100 cm below the sediment-water interface based on a study conducted on a similar SMI from a California continental margin setting (Harrison et al., 2009). The sulfate-methane interface is further defined as existing underneath sulfate-bearing sediment but above sulfate-depleted, methane rich sediment, where methane and sulfate are consumed and dissolved inorganic carbon (DIC) and hydrogen sulfide (HS-) are produced (Ussler 2003). This interface may have been at a different depth in the Cretaceous when the Tepee Buttes seeps were forming, which could account for some of the variations in composition and texture. The precipitated structure begins to accumulate subsurface and, in the case of the Pillar Rock, forms the base of the chimney structure. Inclusion of a significant siliciclastic component lends itself to the hypothesis that the initial building block of the micritic peloidal matrix blobs formed from the influence of pore water in this shallow surface sediment area (between 10s to 100s of centimeters below the sediment-water interface and the sulfate-methane interface). Local siliciclastics were thus incorporated as a partial component of the pelmicrite that makes up most of the micritc peloidal matrix blobs. The Tepee Buttes showed a similar terrigenous component, indicating that the Cretaceous seep sites also incorporated siliciclastic material from the surrounding Pierre Shale as they formed within the sediment. The Pillar Rock had larger grain sizes ranging from roughly 0.2mm to 0.5mm in width, also indicating a subsurface mode of formation that led to incorporation of seafloor material. Similar instances were seen in the Tepee Buttes with grains (~0.01-0.2mm width) of siliciclastic material noted within the primary micritic fabric, which is direct evidence for a subsurface mode of formation (Figure 12). Differences in siliciclastic grain sizes is likely due to the greater degree of diagenesis in the Tepee Buttes samples, which would account for the smaller grains. Figure 32 shows the proposed method of initial formation of the Pillar Rock and Tepee Buttes within the

sediment. In this model, 1) seep rock forms subsurface through microbial mediation, 2) incorporates siliciclastic material, and 3) is later exhumed above the sediment-water interface where it undergoes its initial stage of diagenesis. During this stage, cementation via botryoidal calcite begins in pore spaces within the rock created by abandoned conduit and boring holes.

The more negative carbon isotope signatures of the Pillar Rock and the Tepee Buttes rocks confirms a substantial influence from anaerobic methane oxidation in addition to sulfate reduction that is occurring closer to the sulfate-methane interface within the sediment. Since both the ancient (Tepee Buttes) and modern (Pillar Rock) samples have similar signatures, on the most basic level, it seems that these rocks formed at sites that had similar microbially mediated origins. Based on the results obtained from this study, it appears that despite the existence of distinct decimeter-scale blebs that have likely accreted together to form the Pillar Rock, the internal fabric types are mostly constant with little variation in texture - minus the relative porosity - and little variation in color. With the blue and white mottled/ finely alternating texture as the dominant type, it is likely that this type is precipitated via anaerobic oxidation of methane coupled with sulfate reduction. Two values, which are slightly less negative than the other values (-34.5 and -33.6) can be explained by the difference in porosity at these sites. The connections between slightly less negative $\delta^{13}C$ signatures and the more porous/ highly cemented locations on the Pillar Rock samples seems to indicate that these are areas of lower density of bacteria. The areas of more coherent cementation that also showed abundant evidence of pyrite framboids (framboids are good indicators of the presence of sulfate reducers; Mozer 2010) have more negative $\delta^{13}C$ signatures and could be representative of areas that have more bacteria involved in the precipitation of carbonate. Alternatively, the areas that are more porous perhaps represent slightly older areas of initial, microbially-mediated carbonate growth that was previously much

denser but was in a semi-active to active process of being dissolved and perhaps existed closer to the sediment-water interface than the sulfate-methane interface. Through being partially dissolved, the microbial signatures for these areas could have been slightly overprinted.

Pores in the Pillar Rock and the Tepee Buttes are also of importance to distinguishing the methods of forming seep rock. The large number of conduits in the Pillar Rock suggests that there is no central conduit that supplies the hydrocarbons in seep environments. Thus, the random occurrence of conduit holes suggests that hydrocarbon seepage is diffuse. Many additional pores exist that appear to be from the boring of organisms into the hard substrate. This formation is likely between primary and secondary and partially happens post-exhumation. The Tepee Buttes rock likely also had these types of holes but the additional diagenesis the rock has undergone makes it difficult to distinguish differences between pore spaces. The void spaces that have been distinguished in thin section likely were pore spaces that existed in the primary fabric and were further dissolved through later diagenetic events.

Diagenesis/ Formation Post-Exhumation

Diagenesis is apparent in the existence of allochems and cements that are abundant in the Tepee Buttes. Allochems tend to have an adundance of peloids with rims of isopachous cement surrounding them as well as bits of the original micrite and are further cemented together with later yellow calcite and botryoidal calcite. The occurrence of peloids within the allochems suggests that they are not simply reworked bits (intraclasts) of the original fabric type that formed via the initial output of hydrocarbons. The allochems likely have a later origin due to the observation that they tend to fill in cracks and pore spaces (Figure 20A). The origin of the holes/cracks and subsequent peloidal (allochem) infillings is still up for debate. It has been suggested (personal communication with Bruce Simonson) that they could be boring holes that

caused bits of the original rock material as well as fecal pellets to fill in the spaces post-boring. I have not found sufficient evidence to support this idea yet and for the purposes of this paper, continue to propose that they are likely former conduit holes that have undergone dissolution through diagenetic events, making the voids sufficiently large for allochem material to be transported in by marine or other waters.

It must also be noted that differences in the abundance of peloids and clams within the Pillar Rock versus within the Tepee Buttes rocks also point to rather significant differences in environments for the two sites. Pillar Rock samples tended to have only a few occurrences of small lucinid bivalve shells, and peloids were also generally smaller and contained within specific layers of the micritic material. In contrast, the Tepee Buttes rock often had abundant occurrences of lucinid bivalve shells, distinct areas of cemented peloids with isopachous rims and areas of loose, "free-floating" peloids. The cemented peloids (allochems) represent a well-sorted fabric in which individual peloids had sufficient time to develop isopachous rims of calcite growth within marine waters. These likely accreted together in a later event and were cemented by yellow calcite to form the observed allochem structure that was then later washed into a void space. These fabrics could have formed subsurface and from the influence of marine waters (indicated by the isopachous rims), but after the initial formation of the micritic matrix building block and some diagenetic event that caused dissolution of pore spaces. Later stage loose peloids are part of an unsorted section of material and thus must have come after the cemented peloidal fabric, indicating a connection to the surface at this time. The differences in stages of peloid occurrence also possibly suggests two different stages of allochems, a pelbiosparite allochem with looser, well-sorted peloids and the pelmicrite allochem that is well cemented with matrix and may have independent peloids (Figure 20).

34

Diagenetic changes were inferred in the Tepee Buttes samples based on textural observations and stable isotopes for specific sites within the samples. Three main stages were noted: the first stage of diagenesis is the formation of isopachous rim cement and yellow calcite cement, the second is a development of sparry calcite within pore spaces, and the third stage is a replacement of bivalve shell carbonate with blocky calcite. Several instances of fractured, isopachously-rimmed peloids were found that typically had the sparry calcite growth through the fracture space (Figure 33), indicating that the spar textures were likely later stage events. It is unclear which of the sparry calcite stages happened first but results of luminescence and isotopes show that they are separate fabric types. These diagenetic events are possibly explained by a variation in source fluid over time or differences in rate of mixing between source fluid and seawater/porewater.

Oxygen isotopic signatures from Butte 326.5 and Butte 710 ranged from -2.9 to -12.2 ‰ VPDB. Due to the easily overprinted nature of oxygen isotopic values from the influence of reworking through tectonics and subsequent diagenetic events, it is likely that these values were more similar to the Pillar Rock when these seep sites were of the same approximate age. Without further analysis however, I cannot fully confirm or deny this hypothesis. Another large drawback in attempting to make comparisons between these ancient and modern seep sites is that the environments of formation for each were slightly different in terms of water depth and temperature of formation. The Western Interior Seaway in which the Tepee Buttes seeps formed was likely at much shallower and warmer environment than that of the Gulf of Mexico (Pillar Rock site) at roughly 4°C.

Evidence of significant diagenetic events was noted in the Tepee Buttes rocks by the carbon isotopic signatures found connected to specific fabric types. There was a substantial

difference between allochem (with yellow calcite) versus micrite fabric versus the sparry calcite. Values in the -30 to -32‰ range from the allochem to micrite fabric indicate a substantial influence of sulfate reducing microbes and methane-oxidizing Archaea. Values in the -12 to -24‰ ranges that were noted in the sparry calcite areas indicated no influence of methane-oxidizing Archaea and a small contribution from sulfate reducing microbes. This indicates that the later stage cement growth was likely taking place closer to the sediment surface or possibly within the water column and that the seep site was no longer located at the depths within the sediment that it had been at the time of the precipitation of the yellow calcite cement (i.e. the first stage of cement precipitation). The higher values of carbon and oxygen isotopes recorded for one sample of spar indicate a stage of cement growth that is likely associated with a vug filling diagenetic event (Spar 1). The less negative carbon isotope values in the -20s represent a different diagenetic event that is associated with cement growth in cracks, and void spaces left by the dissolution of bivalve shell fragments that were included in the cementation process (Spar 2). Amongst the spar samples, a difference in spar growth stages was noted via luminescence spectroscopy that confirms stage differences.

Significant differences in luminescence between the Gulf of Mexico samples and the Tepee Buttes samples are indicative of the constituent minerals in each of these sites, and of the difference in diagenesis between the samples. The GOM samples showed extremely weak to no luminescence throughout the samples. One definitive conclusion that can be made from the lack of luminescence in both rocks, is that the phases of carbonate formation in these rocks are not significant or dispersed far enough apart in a temporal scale to exhibit significant differences, i.e. the Pillar Rock has not undergone sufficient diagenesis to cause visible luminescence. This confirms that the Pillar Rock is still geologically young rock in which carbonate minerals have

not undergone recrystallization events during which impurities could be introduced that would luminesce.

The Tepee Buttes samples, however, did exhibit a fair amount of luminescence. The most significant finding from the photographs taken under the CL scope was the confirmed existence of two distinct stages of sparry calcite cementation. The first fabric type, noted as Spar 1 (void-filling spar) shows significant deep red luminescence with some sections exhibiting a banding texture of alternating dark and red luminescence within the sparry calcite zone. Other zones, referred to as Spar 2 (bivalve filling spar), did not show much luminescence beyond a faint dark brown glow. The differences between these two types of spar that otherwise look as though they are part of the same phase in cross-polarized light under a normal petrographic microscope, indicate that they are actually not part of the same carbonate growth phase. It is far more likely that these different cement phases are representative of distinct diagenetic events. I propose that Spar 2 represents an infilling from vadose/meteoric waters after the original aragonite shell of the bivalve had been dissolved, that led to a relatively quick precipitation of secondary calcite. It is unclear whether this event occurred before or after a similar but separate diagenetic event that caused the precipitation of the Spar 1 calcite in the void spaces. I can, however, propose that an initial phase of cementation with botryoidal growth occurred before both Spar 1 and Spar 2 cementation events as represented by its distinct carbon isotope signatures, its orientation near pyritic framboids, and its appearance as a crosscut fabric type in some areas.

The pyrite framboids in the Tepee Buttes, noted earlier in the discussion, were also found to mostly exist near the edges between the micritic peloidal matrix and the second stage sparry calcite (bivalve shell filling; Figure 18 A&B) and the zones of botryoidal calcite void fillings (Figure 22 C), perhaps indicating that microbes preferentially accumulate around the perimeters

of pore/ void spaces and aid in the nucleation of cements into void spaces, similar to what is currently happening in the Pillar Rock. At the interface between these two zones, also existed a potential sulfate reduction zone that left evidence of its existence in the form of dark staining that appear opaque in crossed polars. This zone, apparent around areas of more nearly circular voids, is hypothesized to indicate a former conduit hole that at some point, had hydrocarbon seepage running through and that left a rim of staining around the edge. The presence of the hydrocarbons could have allowed for the existence of a higher density of microbes such as the sulfate reducers that would have precipitated pyritic compounds, leading to the dark appearance of the rims in thin section.

If bacteria/ microbes begin to accrete around areas of weakness in the Pillar Rock matrix, then a similar scenario could come into play with these microbes preferentially forming nucleation sites around zones of weakness in the young Tepee Buttes. The presence of the nucleation sites coupled with possible exhumation and exposure to seawater could have produced the conditions needed to begin the precipitation of botryoidal crystal growth (a process that can happen fairly rapidly; Mohomad & Tucker, 1992). This seems to perhaps be confirmed by the less negative signatures that could have come about by inclusion of seawater in the locations sampled. If the growth of these botryoidal crystals proliferated, they could have also led to an increase in the creation of fissile cracks in the micritic matrix that could have led to further botryoidal crystal growth (acting as positive feedback loop).

Ultimately, the Pillar likely underwent exhumation at some time and subsequently rose above the sediment water interface where it began to undergo diagenesis through the influence of marine waters and was subject to intense boring from associated fauna that benefited from its existence above the surface. It is also likely that some amount of excavation by circular currents

led to the sediment being washed away from the area surrounding where the Pillar was forming subsurface. Due to the size and height of the pillar, however, this process likely could not account for the entirety of its exposure above the surface. Therefore, I propose that the Pillar began forming within the subsurface and was later exposed through a combination of uplift, exhumation, and deep-water current action. Post-exhumation, a negligible amount of precipitation of carbonate occurred while diagenetic processes likely took over. I propose that a similar initiation of thin-section scale structures that formed in the Gulf of Mexico at the Pillar Rock site also occurred within the Western Interior Seaway to begin the formation of the Tepee Buttes. After the Laramide Orogenic event that led to the uplift of the surrounding area and the phasing-out of the seaway, these seep structures were exposed to seawater, then burial, and finally sub-aerially exposed fairly recently. During the period of influence of seawater, there was dissolution in the rocks seen as the pore spaces (that have later been filled in with allochems and cement). Continued tectonics exposed these seep sites to vadose and meteoric waters that led to a general precipitation of various cement types (later stage botryoidal cements and sparry calcite cements).

CONCLUSION

In summary, this study reveals several conclusions about hydrocarbon seep rocks:

1. Initial formation of carbonate occurs through the mediation of several different active microbes that fix carbon through a series of known chemical reactions. This process

typically occurs within the sediment, somewhere between the sulfate-methane interface and the sediment-water interface.

2. The main microbes that help form seep rock (i.e. the Pillar Rock and Tepee Buttes) are sulfate reducers and methane-oxidizing Archaea. More in depth isotopic analysis needs to be conducted to determine the differences between microbes in the Pillar Rock and the Tepee Buttes.

3. Almost immediately after the formation of the initial micritic matrix building blocks within the near surface sediments, cementation by botryoidal calcite begins to occur. As the rock is cemented, it may also experience exhumation. Therefore, primary formation of the seep rock sediments occurs below the sediment-water interface.

4. Post-exhumation of the Pillar Rock (though some amount of exhumation likely continues to be an active process) the conical seep structure is exposed above the sediment-water interface and subsequently undergoes additional diagenesis in the form of further cementation and also erosive processes.

5. The Tepee Butte history includes burial and burial diagenesis not yet experienced by the Pillar Rock.

6. The Buttes underwent diagenesis as they experienced burial, re-exhumation, and other tectonic processes and as a result, were exposed to meteoric and vadose waters that led to the formation of a variety of different cement types as well as stages of cementation.

7. The rapid tectonics of the Western Interior Seaway as well as the location of formation of Buttes rocks within the sediment likely exposed it to a greater degree of initial diagenesis from the influences of seawater, and then an additional component

of late-stage diagenesis that led to overprinting of signatures found in newly forming

seep rocks such as the Pillar Rock. Although it is necessary to account for the

differences in oxygen levels, temperature of seawater, and depth below the surface in

both sites, it is possible that the Pillar Rock could undergo a similar sequence of

events and that it represents a roughly similar initial starting point for the formation of

the Butte seep site rocks. Thus, looking at the sequence of formation from Pillar

Rocks to Buttes provides a rough approximation of the evolution of a hydrocarbon

seep site over geologic time.

REFERENCES

Aharon, P. (1994). Geology and biology of modern and ancient submarine hydrocarbon seeps and vents: An introduction. *Geo-Marine Letters, 14*, 69-73.

Aharon, P. (2003). Is Drilling in Deepwater Gulf of Mexico Uncorking Bad Genies? *GCAGS/GCSSEPM Transactions, 53.*

Anderson, J. (2006). *Petrologic and Petrographic Analysis of Ancient Submarine Hydrocarbon Seep Deposits (Late Cretaceous) from the Tepee Buttes of Colorado* (Bachelor of Arts).

Bailey, J. V., Orphan, V. J., Joye, S. B., & Corsetti, F. A. (2009). Chemotrophic Microbial Mats and Their Potential for Preservation in the Rock Record. *Astrobiology, 9*(9), 843.

Bian, Y., Feng, D., Roberts, H. H., & Chen, D. (2013). Tracing the evolution of seep fluids from authigenic carbonates: Green canyon, Northern Gulf of Mexico. *Marine and Petroleum Geology, 44*(0), 71-81.

Campbell, K. A., Farmer, J. D., & Des Marais, D. (2002). Ancient hydrocarbon seeps from the Mesozoic convergent margin of California: Carbonate geochemistry,fluids and palaeoenvironments. *Geofluids, 2*, 63-94.

Campbell, K. A. (2006). Hydrocarbon seep and hydrothermal vent paleoenvironments and paleontology: Past developments and future research. *Palaeogeography, Palaeoclimatology, Palaeoecology, 232*(2-4), 362-407.

Enning, D. & J. Garelfs. (2014). Corrosion of Iron by Sulfate-Reducing Bacteria: New Views of an Old Problem. *Applied and Environmental Microbiology, 80* (4), 1226-1236.

Folk, R. (1962). Spectral Subdivisions of Limestone Types. *American Association of Petroleum Geologists, 1*, 62-84.

Foucher, J. P., G. K. Westbrook, A. Boetius, S. Ceramicola, S. Dupré, J. Mascle, J. Mienert, O. Pfannkuche, C. Pierre, & D. Praeg. (2009). Structure and Drivers of Cold Seep Ecosystems. *Oceanography, 22* (1), 92-109.

Fu, R., A. D. Del Genio, & W. B. Rossow. (1994). Influence of Ocean Surface Conditions on Atmospheric Vertical Thermodynamic Structure and Deep Convection. *J. Climate, 7*, 1092-1108.

Harrison, B. K., H. Zhang, W. Berelson, & V. J. Orphan. (2009). Variations in Archaeal and Bacterial Diversity Associated with the Sulfate-Methane Transition Zone in Continental Margin Sediments (Santa Barbara Basin, California). *Applied and Environmental Microbiology, 75 (*6), 1487-1499.

Hiatt, E. E. & P.K. Pufahl. (2014). Cathodoluminescence Petrography of Carbonate Rocks: A Review of Applications for Understading Diagenesis, Reservoir Quality, and Pore System Evolution. *Mineralogical Association of Canada Short Course 45.* 75-96.

Kauffman, E.G. (1984). Paleobiogeography and evolutionary response dynamic in the Cretaceous Western Interior Seaway of North America. In Westermann, G.E.G. (ed.), *Jurassic-Cretaceous Biochronology and Paleogeography of North America: Geological Association of Canada, Special Paper 27*, 273-306.

Kauffman, E. G., Arthur, M. A., Howe, B., & Scholle, P. A. (1996). Widespread venting of methane-rich fluids in Late Cretaceous (Campanian) submarine springs (Tepee Buttes), Western Interior Seaway, U.S.A. *Geology, 24*, 799-802.

Mohamad, A. H. & D. E. V. Tucker. (1992). Diagenetic History of the Aymestry Limestone Beds (High Gorstian Stage), Ludlow Series, Welsh Borderland, U.K.. In K. H. Wolf & G. V. Chilingarian (Eds.), Diagenesis, III (pp. 6-7). Amsterdam: Elsevier Science Publishers.

Mozer, A. (2010). Authigenic pyrite framboids in sedimentary facies of the Mount Wawel Formation (Eocene), King George Island, West Antarctica. *Polish Polar Research, 31*(3), 255-272.

Riding, R. E. (2000). Microbial carbonates: The geological record of calcified bacterial-algal mats and biofilms. *Sedimentology, 47*(1), 179-214.

Roberts, H. H., & Aharon, P. (1994). Hydrocarbon-derived carbonate buildups of the Northern Gulf of Mexico continental slope: A review of submersible investigations. *Geo-Marine Letters, 14*, 135-148.

Shapiro, R., & Fricke, H. (2002). Tepee buttes: Fossilized methane-seep ecosystems. *GSA Field Guide Publications.*

Shapiro, R. (2000). A Comment on the Systematic Confusion of Thrombolites. *Palaios, 15*, 166-169.

Stolz, J. F. (2000). Structure of Microbial Mats and Biofilms. In R. E. Riding, & S. M. Awramik (Eds.), *Microbial Sediments* (pp. 1-8). Berlin: Springer-Verlag.

Treude, T., K. Knittel, M. Blumenberg, R. Seifert, & A. Boetius. (2005). Subsurface Microbial Methanotrophic Mats in the Black Sea. *Applied and Environmental Biology, 71* (10), 6375-6378.

Treude, T., V. Orphan, K. Knittel, A. Gieseke, C. House, & A. Boetius. (2007). Consumption of Methane and CO2 by Methanotrophic Microbial Mats   from Gas Seeps of the Anoxic Black Sea. *Applied and Environmental Microbiology, 73* (7), 2271-2283.

Ussler, W., C. K. Paull, S. Hallam, E. Delong, Y. Chen, R. Matsumoto, T. Lorenson, W. J. Winters. (2003). The Anatomy of the Sulfate-Methane Interface in a Methane-Rich Core From the Gulf of Mexico. *GSA Abstracts with Programs, 35* (6), 287.

FIGURES AND TABLES

EXAMPLES OF DOCUMENTED METHANE-SEEP CARBONATES

Age	Location	Tectonic Setting	Reference
Recent	**Gulf of Mexico**	**Continental slope**	**Neureauter & Roberts, 1994**
Recent	Oregon Offshore	Subduction zone	Kulm et al., 1986
Recent	Denmark Offshore	Continental shelf	Jensen at al., 1992
Recent	North Sea	Continental shelf	Hovland et al., 1987
Recent	Japan Offshore	Subduction zone	Sakai et al., 1992
Recent	Blake Ridge	Continental shelf	Naehr et al., 2000
Recent	Northern California	Continental margin	Levin et al., 2003
Miocene	Monferrato, Italy	Foredeep basin	Clari & Martire, 2000
Oligocene	Washington	Continental shelf	Goedert & Campbell, 1995
Oligocene	Washington	Continental shelf	Squires, 1995
Eocene	Washington	Continental shelf	Geodert & Squires, 1990
Cretaceous	**Colorado**	**Intracratonic sea**	**Kauffman et al., 1996**
Cretaceous	Canadian Arctic	Half-graben	Beauchamp & Savard, 1992
Jurassic	Alexander Island, Antarctica	Forearc basin	Kelly et al., 1995
Proterozoic	Yangtze Gorges, South China	Cap carbonate	Wang et al., 2008

Table 1 Locations of known hydrocarbon seep sites, both modern and ancient. Sites surveyed in this study come from the sites in bold from the recent Gulf of Mexico and the Cretaceous Tepee Buttes (modified from Shapiro & Fricke, 2002).
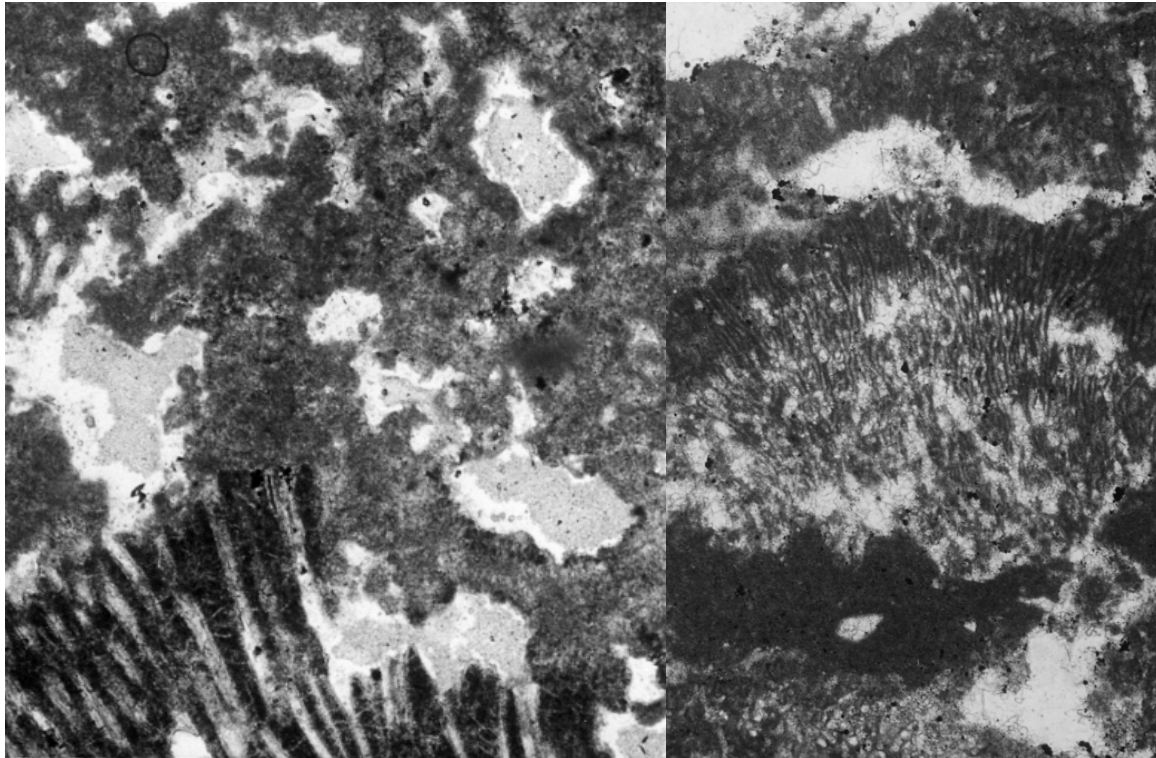
Figure 1 Photomicrographs of clotted thrombolitic to stromatolitic texture commonly seen in microbially produced calcite rock. From Riding's (2000) study of cyanobacteria mats from Greece (left) and Scotland (right).

Figure 2 Map of Gulf of Mexico seep sites focused on in this study. Image adapted from www.nature.org.
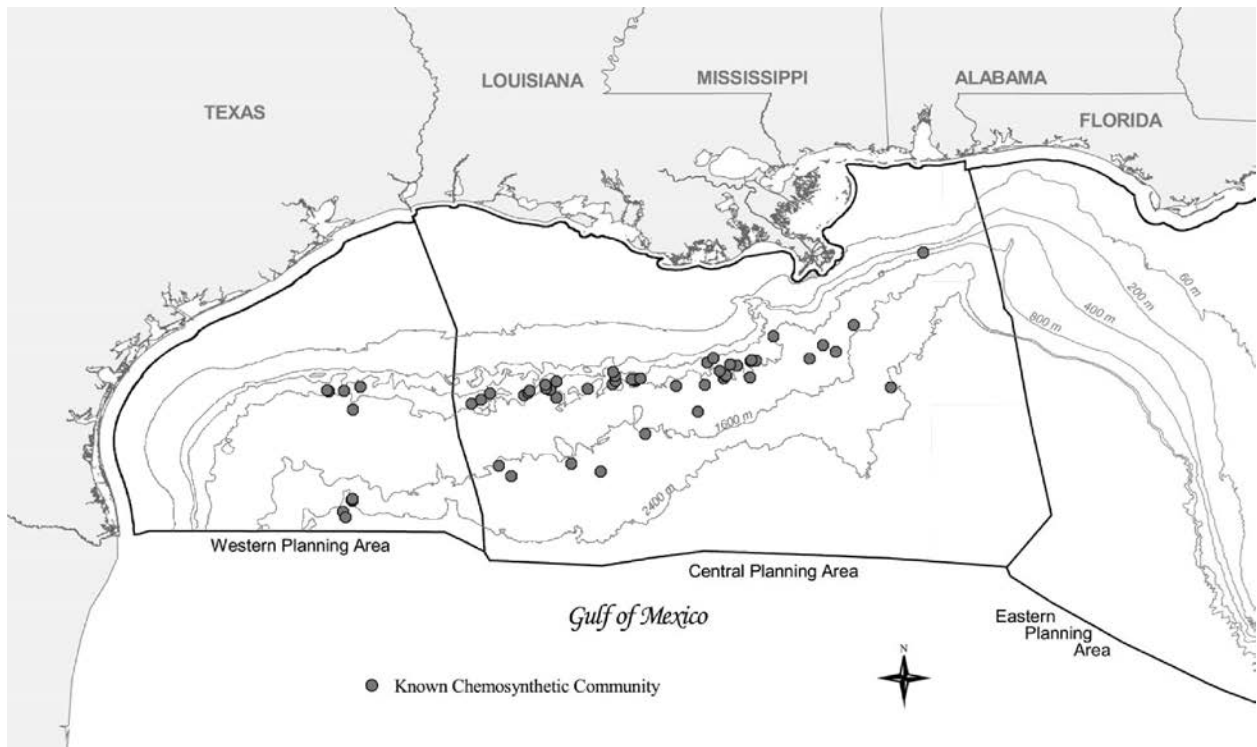
Figure 3 Map of known chemosynthetic communities (thought to be associated with hydrocarbon seepage) in the Gulf of Mexico. Sites used in this study are from the Central Planning Area (map from Minerals Management Service, 2007-2012).

Figure 4 Map of the Western United States during the Late Cretaceous period in which the majority of the hydrocarbon seep sites formed. As the Western Interior Seaway (depicted on the right of the diagram in light blue and centered on Colorado) receded and natural weathering occurred over time, the Tepee Buttes were exposed to show the present-day surface. Picture acquired from the Wisconsin Geosciences webpage - http://www.geoscience.wisc.edu/~chuck/Classes/Mtn_and_Plates/mtns_westernUS.html.
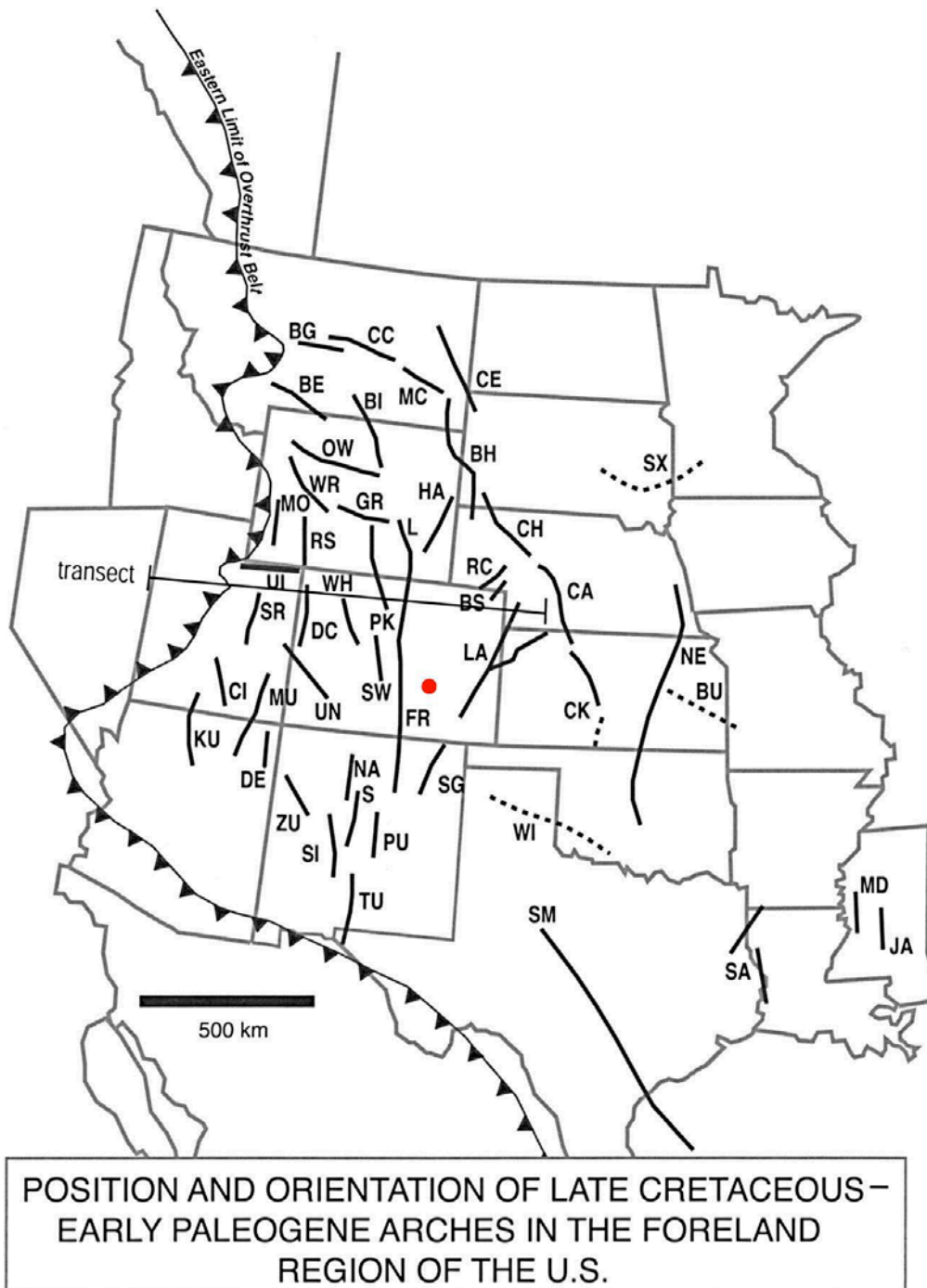
Figure 5 Map of the Laramide Orogenic Faults in the Late Cretaceous. The line labelled FR that cuts through Colorado refers to the Front Range Uplifts, which are related to tectonics that caused the Tepee Buttes formations (red dot). Map from http://rmg.geoscienceworld.org/content/36/1/13/F2.expansion.html.

Figure 6 (A) Oblique aerial view of the Tepee Buttes, CO. Dome-like structures represent the Buttes with high tension electricity poles for scale (Photo by R. Shapiro). (B) Field photograph of a typical Butte structure that has been greatly weathered and overgrown with vegetation. Rock hammer for scale (Photo by K. Parsons-Hubbard).

	Over 2/3 Lime Mud Matrix				Subequal	Over 2/3 Spar Cement		
Percent Allochems	0 - 1 %	1 - 10 %	10 - 50 %	over 50%	Spar and Lime Mud	Sorting poor	Sorting good	Rounded and abraded
Representative Rock Terms	Micrite	Fossiliferous Micrite	Sparse Biomicrite	Packed Biomicrite	Poorly washed Biosparite	Unsorted Biosparite	Sorted Biosparite	Rounded Biosparite
1959 Terminology	Micrite	Fossiliferous Micrite	Biomicrite	Biomicrite	Biosparite	Biosparite	Biosparite	Biosparite
Terrigenous Analogues	Claystone	Sandy Claystone	Clayey or Immature Sandstone			Submature Sandstone	Mature Sandstone	Supermature Sandstone

▪ Lime Mud Matrix ▨ Sparry Calcite Matrix

Table 2 Diagram of the Folk Classification scheme for carbonate rocks. (Adaptation from Folk's 1962 paper; Flugel, 2004).

h

Figure 7 (A) Underwater photograph taken of the Pillar Rock (OCSG) during the 2006 expedition in the Gulf of Mexico. This particular site exhibits a tall chimney-like structure with abundant faunal attachments including a sponge that is apparent at the bottom of the photograph. (B) Cross-section of a sample from the Pillar Rock showing abundance of small conduit holes with stained rims.

A

B
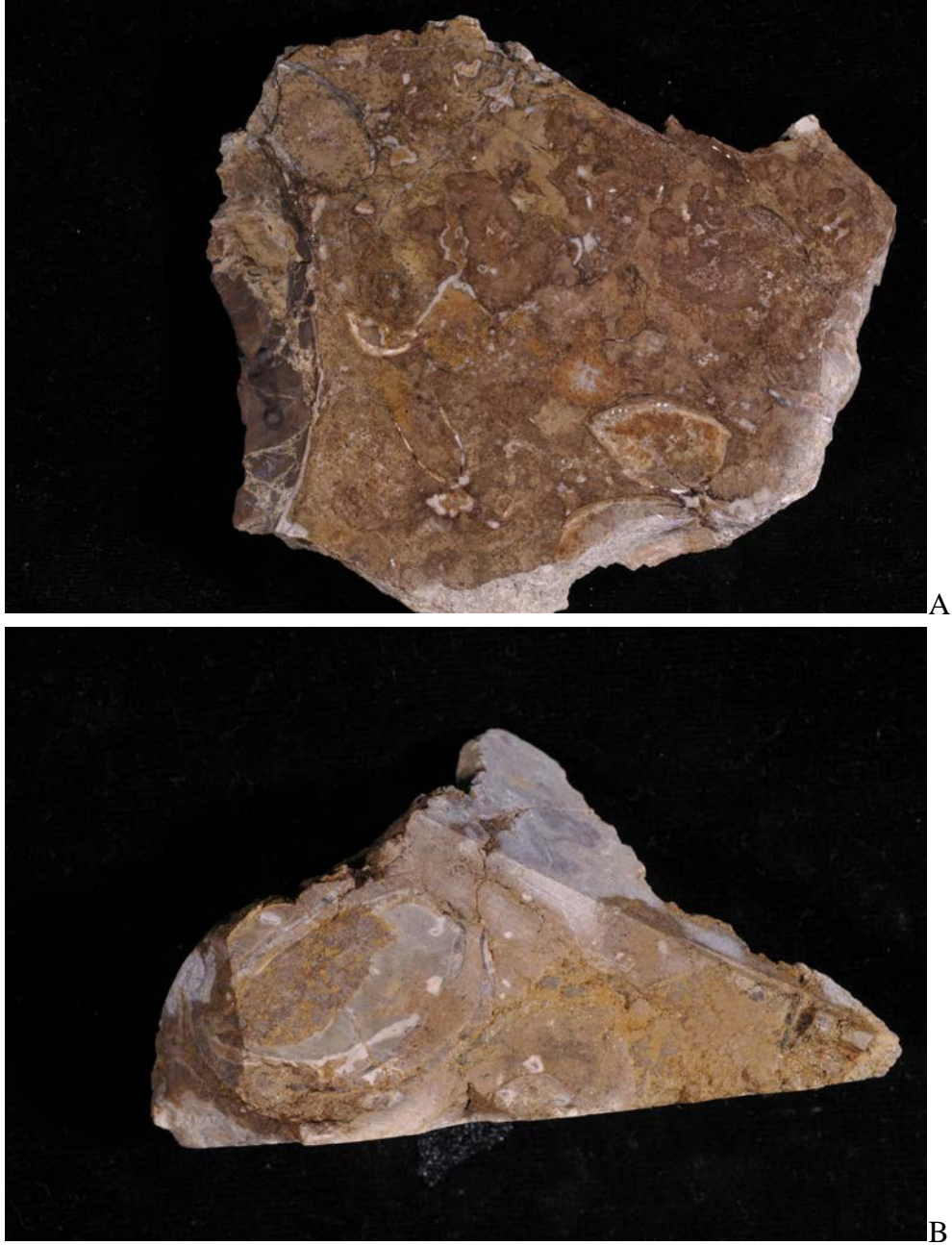
Figure 8 (A) Cross-section photograph of Butte 326.5. (B) Cross-section photograph of Butte 710.
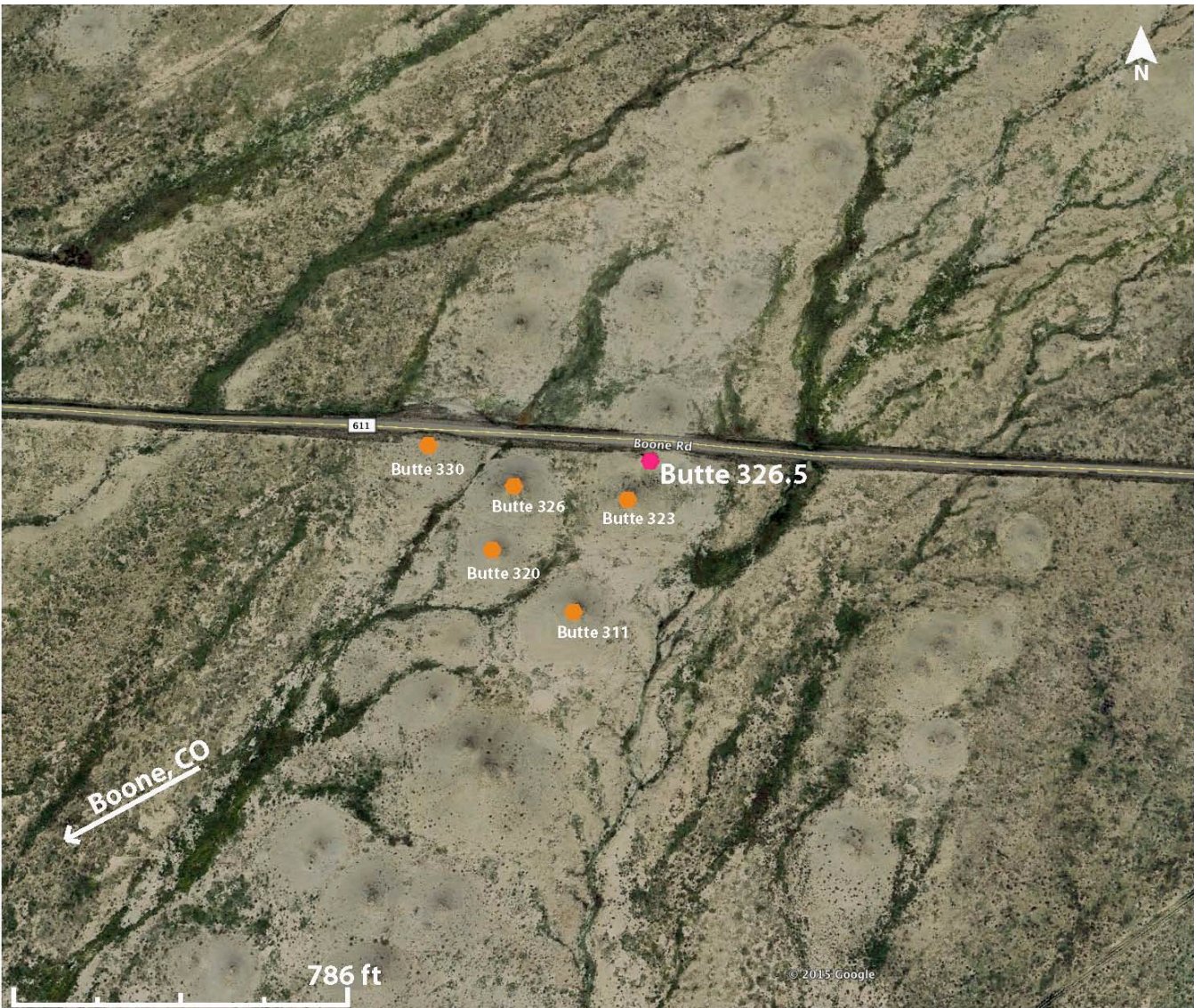
Figure 9 Aerial map of the Tepee Buttes, Boone County Rd cut. Butte 326.5 (represented by the red octagon) and is the main focus from this survey site for the Tepee Buttes samples. (Image from Google Earth 2014; later edited in Adobe Illustrator).
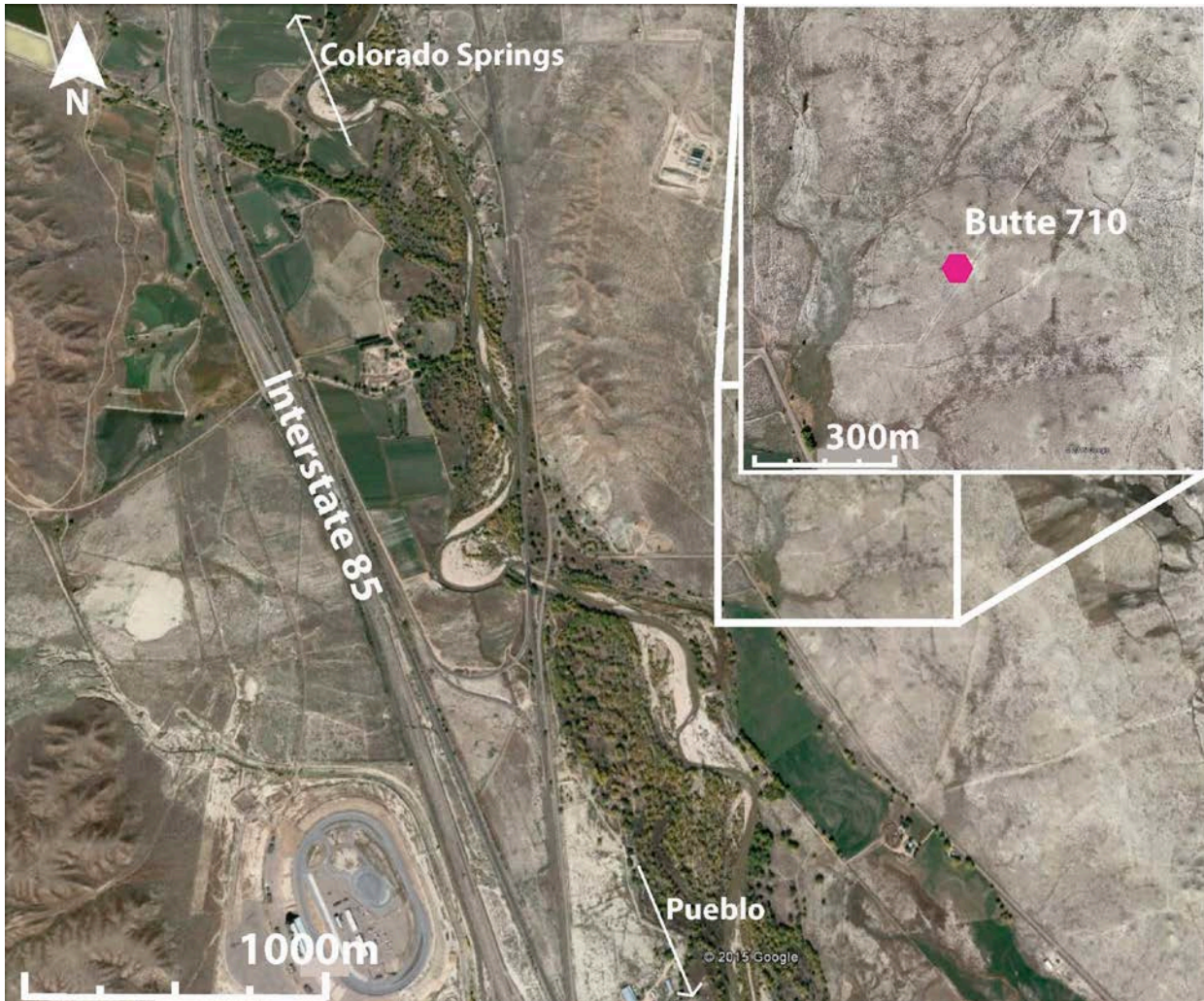
Figure 10 Aerial map of the Tepee Buttes of the North Ranch site (location of Butte 710). Image from Google Earth, 2015; later edited in Adobe Illustrator.

SAMPLES AND METHODS

	Butte #	Point-Counts	Areal %	Acetate Peels	Staining	Digestion	SEM	CL	Stable Isotopes
TPB 002							1 slide - 9 spots		
TPB 003	326.5	2 slides - 25 spots	1 slide - 4 pics	yes	3 pics		2 slides - 47 spots		
TPB 004	658	3 slides - 46 spots	3 slides - 16 pics						
TPB 005	326.5	2 slides - 32 spots	2 slides - 11 pics				1 slide - 20 spots		
TPB 006	736.5	3 slides - 45 spots	1 slide - 7 pics	yes			2 slides - 43 spots		
TPB 007	326.5	1 slide - 18 spots	1 slide - 7 pics			yes		1 slide - 5 pics	hsamp – 5 spots
TPB 008	689	3 slides - 42 spots	3 slides - 15 pics				4 slides - 62 spots		
TPB 009							3 slides - 36 spots		
TPB 014	710		2 slides - 16 pics			yes	1 slide - 7 spots		hsamp – 5 spots
Site									
OCSG83106	Pillar Rock	1 slide - 33 spots	1 slide - 10 pics	yes	yes	yes	2 slides - 25 spots	1 slide - 4 pics	hsamp – 7 spots
OCSG90106	Pillar Rock	2 slides - 53 spots	1 slide - 13 pics			yes			
OCSGB3	Pillar Rock	2 slides - 23 spots	1 slide - 10 pics		yes	yes	1 slide - 9 spots		
GC 272	Green Canyon					yes	4 slides - 64 spots		
GB 425	Garden Banks						3 slide - 33 spots		

Table 3 Run-down of the methods used for each sample. Tepee Buttes samples are listed first, then Gulf of Mexico samples. Samples highlighted in red indicate primary samples used for the bulk of this study.

m

Pillar Rock Samples

Legend:
- Hole/Pore Space
- Micritic Peloidal Matrix
- Botryoidal Cement
- Muddy Accumulated Sediment

11.6%

79.4%

Tepee Buttes Samples

Legend:
- Sparry Calcite Cement
- Allochems
- Hole/ Pore Space
- Micritic Peloidal Matrix
- Botryoidal Cement
- Yellow Calcite

13.6%
23.4%
27.8%
29.2%
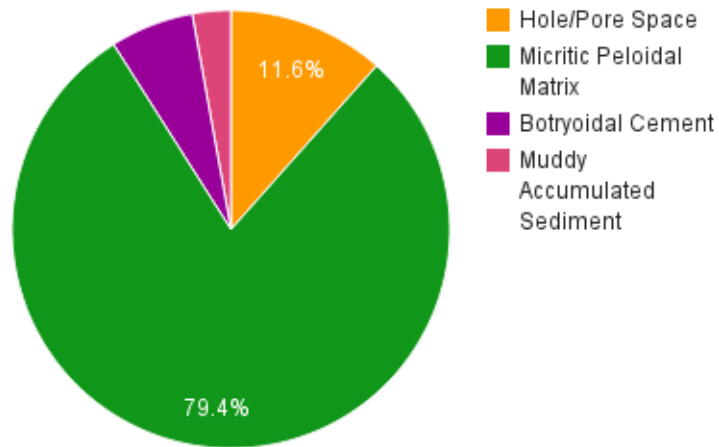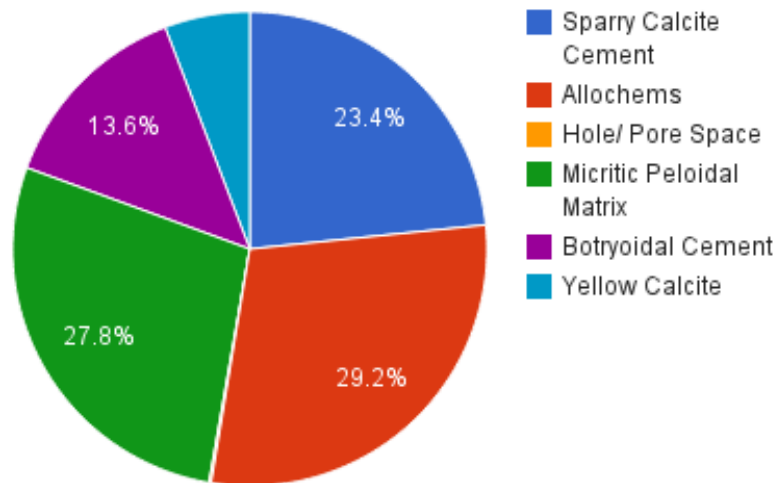
Table 4 Charts of the types of matrix and cement from the two study areas. Chart A shows the Gulf of Mexico (Pillar Rock) samples which are overwhelmingly composed of micritic peloidal matrix. Chart B shows the Tepee Buttes samples, which are fairly evenly split between micrite, allochems, and the sparry calcite cement.

n

Pillar Rock Terrigenous Material	PR 9-1-06	2PR 9-1-06	PR 8-31-06	2PR 8-31-06	OCSG PRB#3	2OCSG PRB#3	Avg of Digested	Stained
%terrigenous	26.67%	17.65%	6.38%	12.82%	18.67%	10.94%	15.52%	12.68%
%carbonate	73.33%	82.35%	93.62%	87.18%	81.33%	89.06%	84.48%	87.32%

Tepee Buttes Terrigenous Material	Butte 710	Butte 014	Butte 002	Avg of Digested
%terrigenous	17.65%	11.30%	15.08%	14.68%
%carbonate	82.35%	88.70%	84.92%	85.32%

Table 5 A table of the percentages of terrigenous material seen in each sample (each of the Pillar Rock samples was calculated twice with similar sized pieces – indicated by the 2 in front of the name). The bulk of data was calculated using the digestion-in-acid method. Stained thin section point counting methods revealed similar values in the Pillar Rock samples.
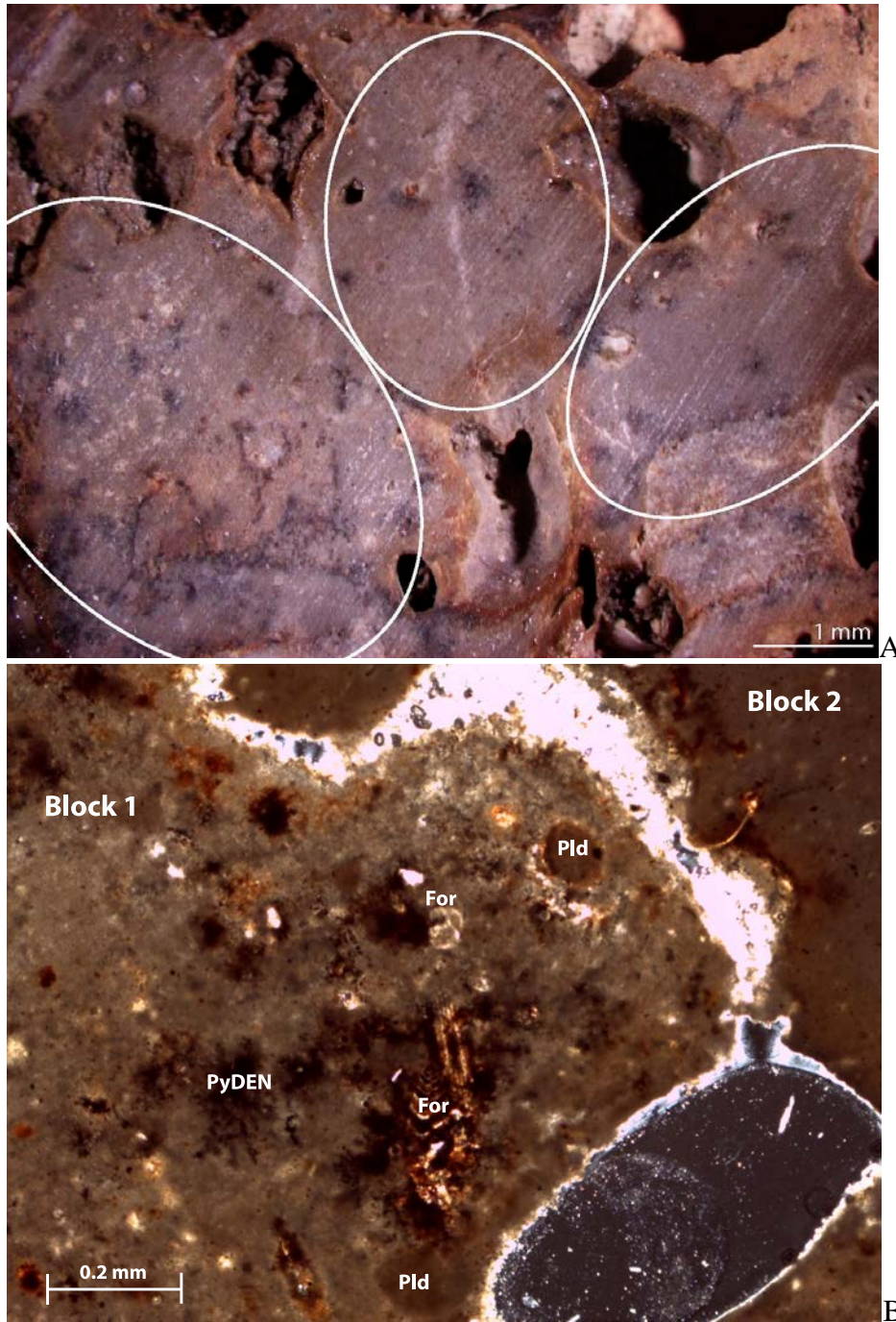
Figure 11 (A) Hand sample picture of distinct blocks that make up the Pillar Rock. Taken at 2.5x Magnification on a Nikon SMZ1500. (B) Thin section photomicrograph of two different blocks (1 & 2). Block one includes pyritic dendrites (PyDEN), foraminifera remains (For), and small peloids (Pld). Taken at 4x magnification.
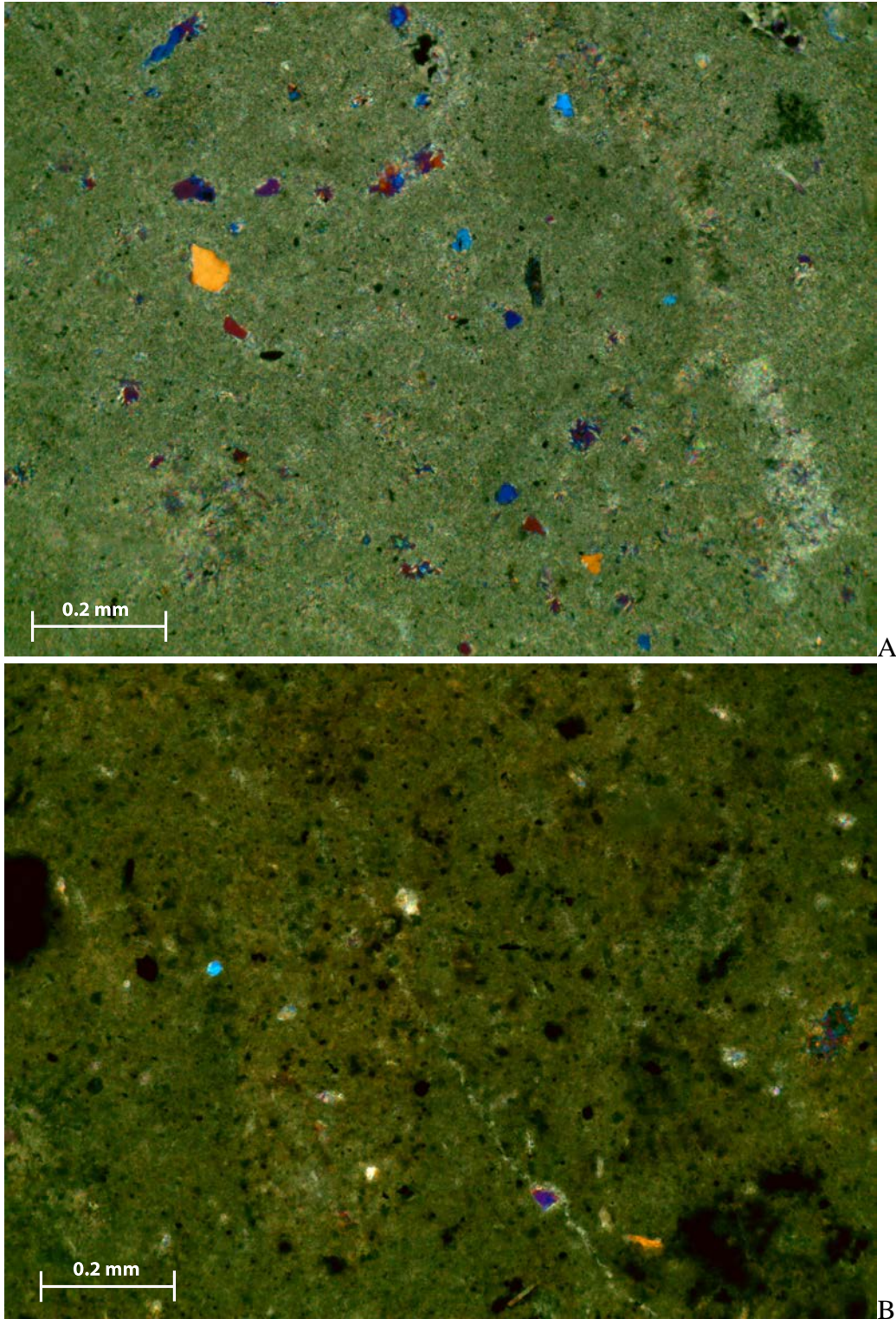
Figure 12 (A) Silciclastic grains in Pillar Rock sample, appearing here as the yellow and blue grains, (B) Siliciclastic grains in the Tepee Buttes (Butte 710), also yellow and blue. Both photomicrographs were taken at 10x magnification in crossed polarized light with the gypsum plate inserted.

q
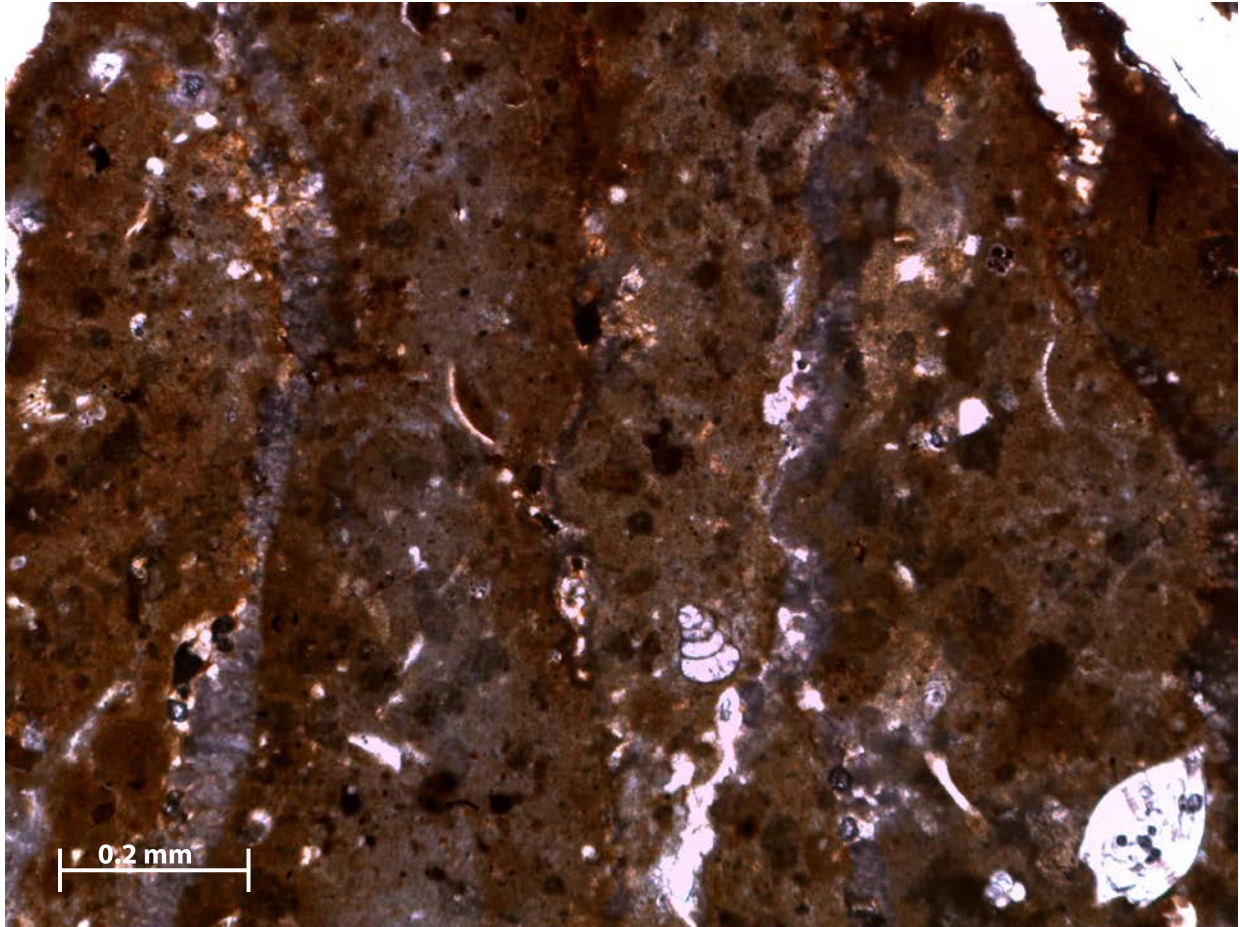
Figure 13 Blue and white alternating mottled texture of the Pillar Rock.
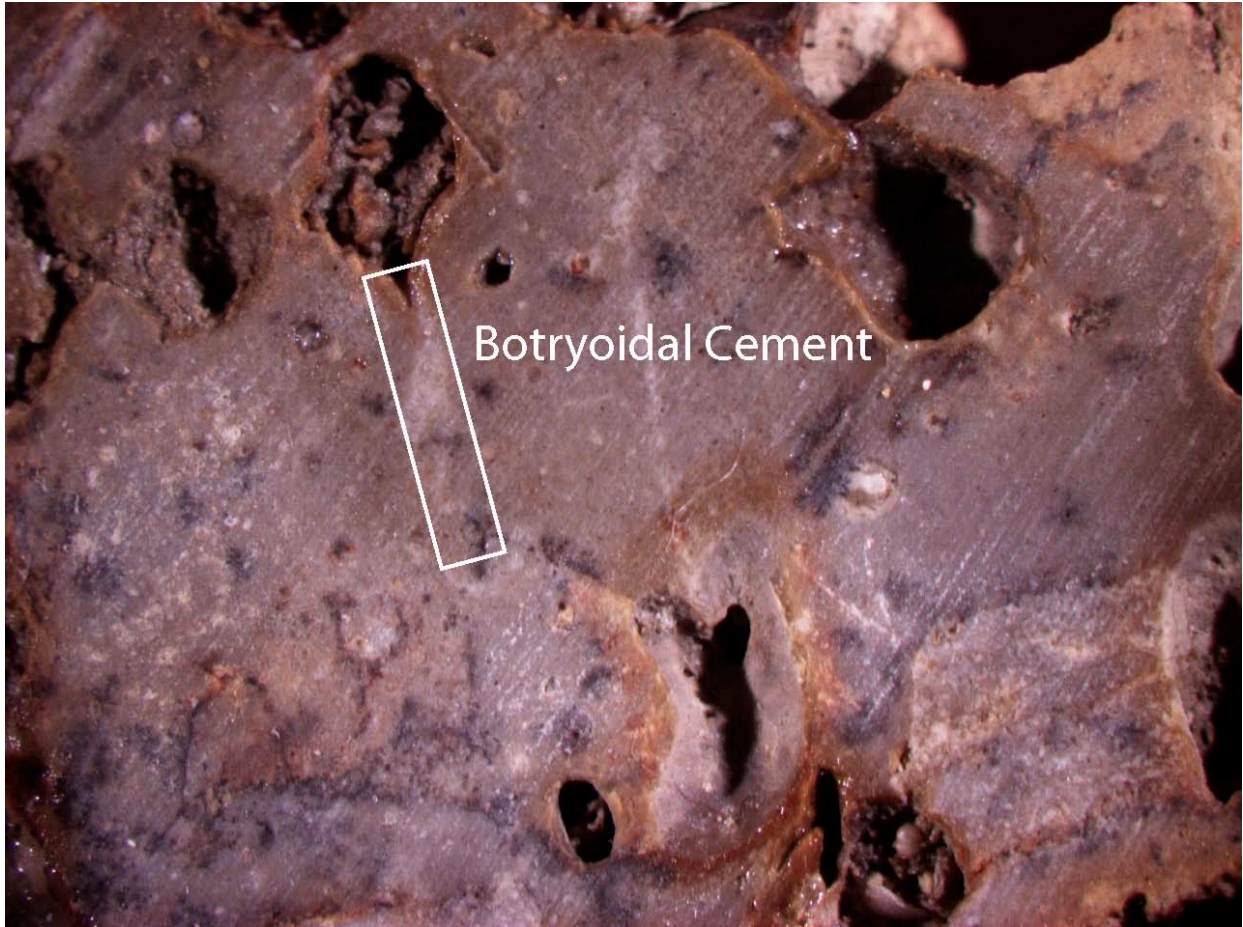
Figure 14 Photograph of Pillar Rock hand sample showing botryoidal calcite cement between blocks. Taken at 2.5x magnification on a Nikon SMZ1500.
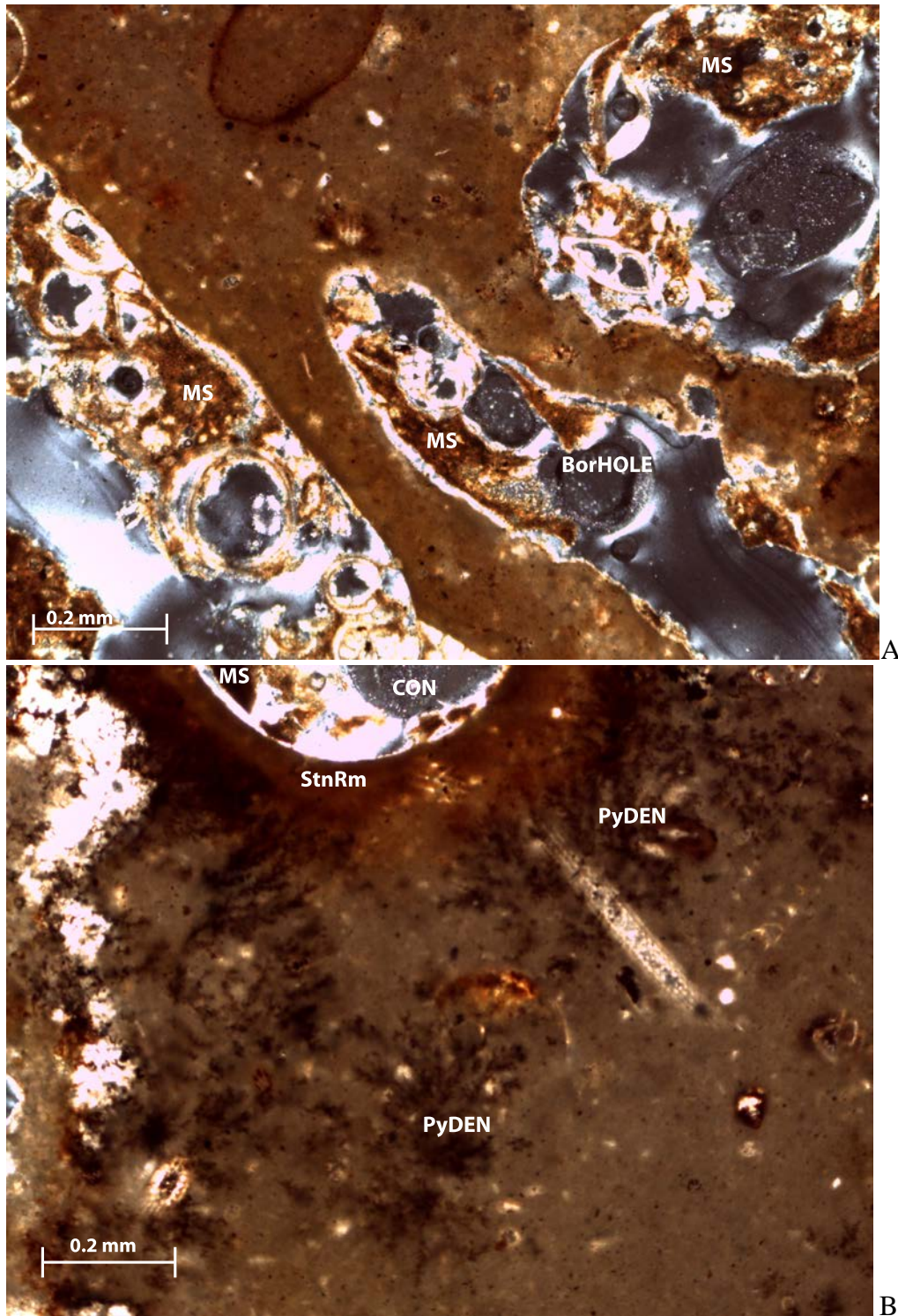
Figure 15 (A) Photomicrograph of a boring hole (BorHOLE) filled with muddy accumulated sediment (MS). (B) Photomicrograph of a conduit (CON), with a concentric rim of staining (StnRm), and muddy accumulated sediment filling. Pyritic dendrites are abundant in the micritic peloidal matrix at this site. Both images taken at 4x magnification.

t

Sample Area	Sample Names	$\delta^{13}C$ (‰ VPDB)	$\delta^{18}O$ (‰ VPDB)
OCSG	PR Galveston_03	-36.6	1.9
	PR Galveston_07	-40.4	2.0
	PR Galveston_04	-34.5	2.2
	PR Galveston_05	-37.9	2.2
	PR Galveston_06	-38.2	2.2
	PR Galveston_01	-37.9	2.2
	PR Galveston_02	-33.6	2.2
Tepee Buttes	TPB 007_05	-22.5	-10.0
	TPB 007_04	-23.1	-10.2
	TPB 007_02	-30.4	-10.6
	TPB 007_03	-31.0	-11.0
	TPB 007_01	-30.5	-12.2
	TPB 014_04	-12.5	-2.9
	TPB 014_02	-37.1	-5.9
	TPB 014_01	-32.1	-9.5
	TPB 014_03	-23.9	-11.3

Table 6 Table of the isotopic data collected for this study, arranged by lowest to highest Oxygen Isotopic values. TPB 007 corresponds to Butte 326.5 and TPB 014 corresponds to Butte 710.

u

Sample Area	Sample Names	δ^{13}C (‰ VPDB)	δ^{18}O (‰ VPDB)
OCSG	PR Galveston_02	-33.6	2.2
	PR Galveston_04	-34.5	2.2
	PR Galveston_03	-36.6	1.9
	PR Galveston_05	-37.9	2.2
	PR Galveston_01	-37.9	2.2
	PR Galveston_06	-38.2	2.2
	PR Galveston_07	-40.4	2.0
Tepee Buttes	TPB 007_05	-22.5	-10.0
	TPB 007_04	-23.1	-10.2
	TPB 007_02	-30.4	-10.6
	TPB 007_01	-30.5	-12.2
	TPB 007_03	-31.0	-11.0
	TPB 014_04	-12.5	-2.9
	TPB 014_03	-23.9	-11.3
	TPB 014_01	-32.1	-9.5
	TPB 014_02	-37.1	-5.9

Table 7 Table of Isotopic data arranged from least to most negative Carbon Isotope signal for comparison. TPB 007 corresponds to Butte 326.5 and TPB 014 corresponds to Butte 710.
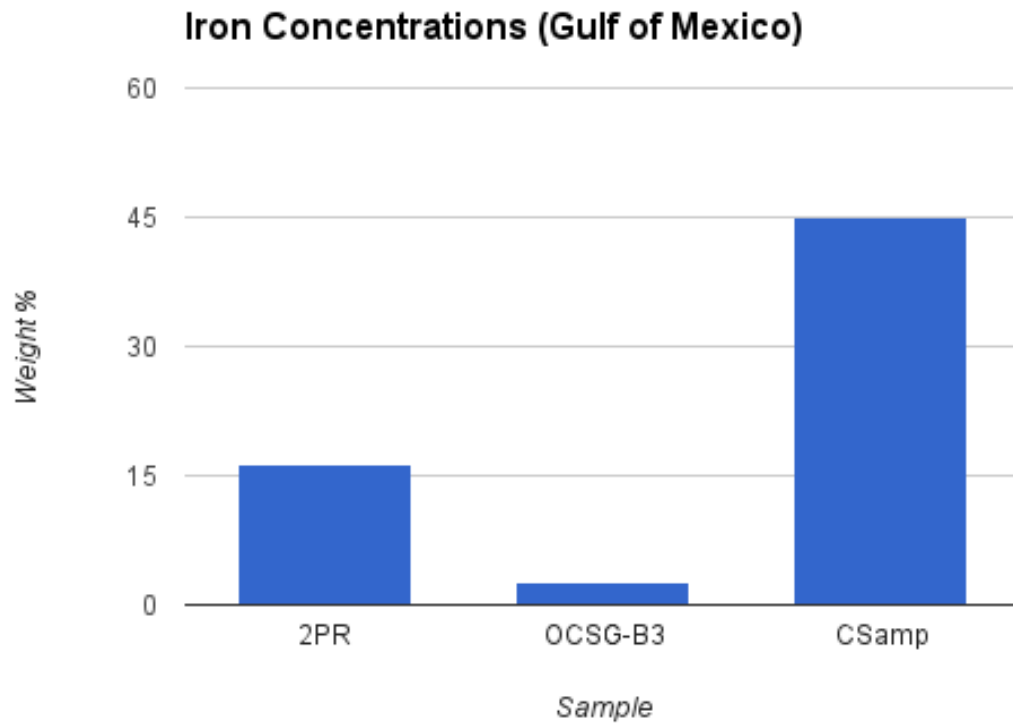
Figure 16 Weight percent iron of Pillar Rock samples obtained using an SEM. Each bar represents the average iron value of many spot analyses for each sample.

X 200   100 um

X 370   50 um
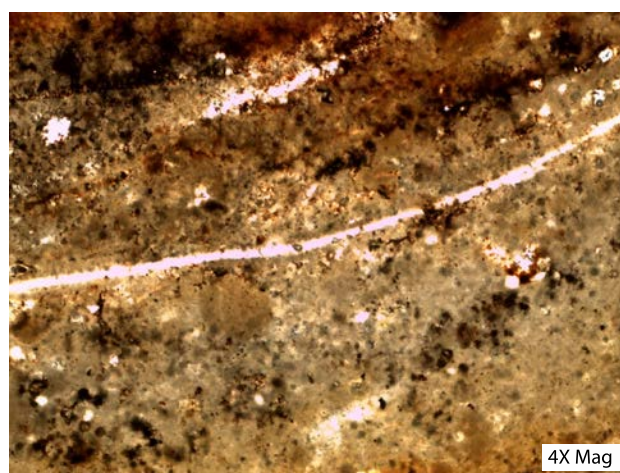
Figure 17 Pyrite framboids found in the (A) Tepee Buttes SEM back-scattered electron image with pyrite framboids represented by the brightest sections, (B) Pillar Rock thin section photo of a planktonic foraminifera with pyrite framboids within secondary pore spaces, (C) Pillar Rock SEM back-scattered electron image, and (D) thin section photograph of Pillar Rock showing the banding of Fe-framboids within the micritic matrix. Framboids are taken to be evidence of sulfate reduction that takes place in both carbonate rock formations.

PyDEN

Spar 2

PyDEN

MicMtx

0.2 mm

A

0.2 mm

MicMtx

PyDEN

PyDEN

PyDEN

Spar 2

B

y

Boty

PyDEN

PyDEN

PyDEN

PyDEN

MicMtx

0.2 mm

C
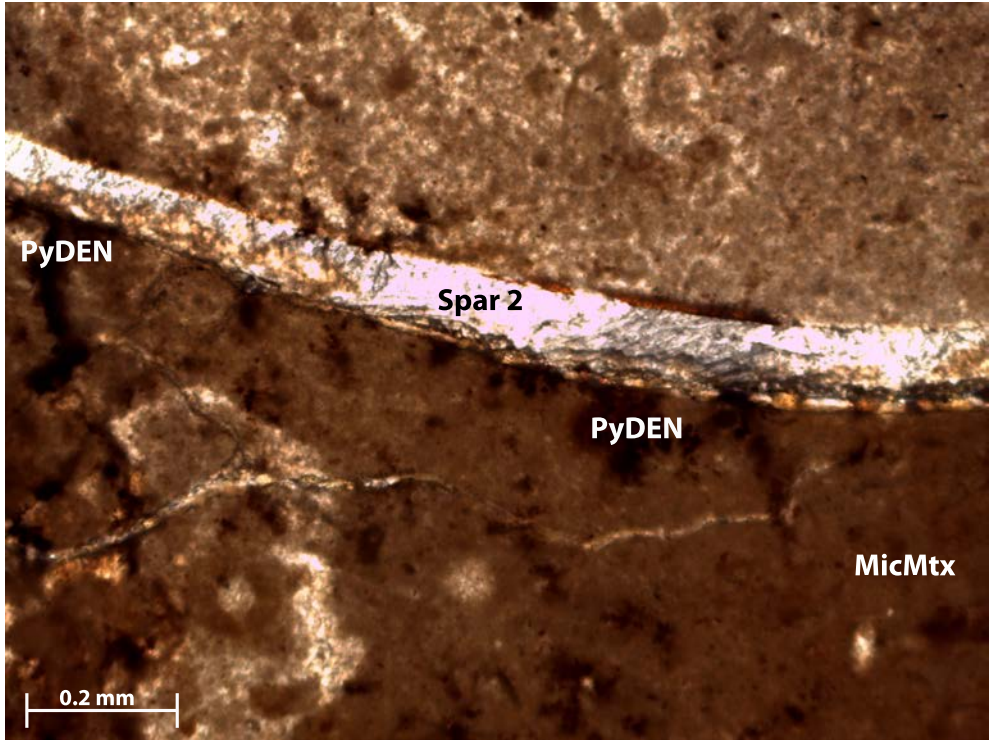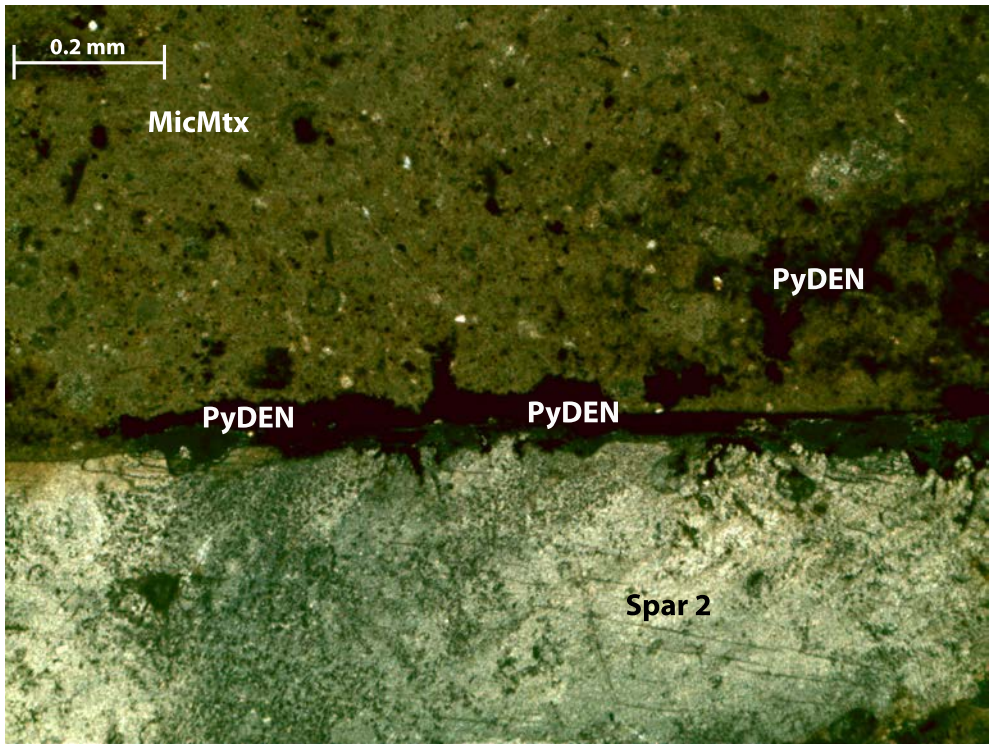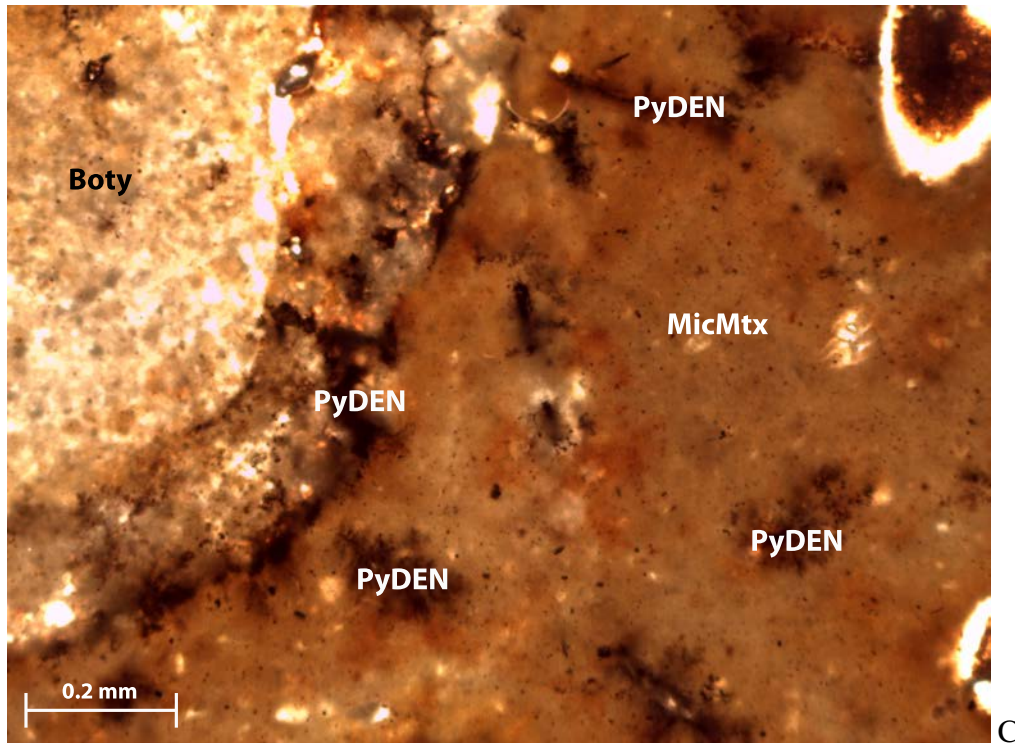
Figure 18 Thin section photomicrographs showing the boundaries between micritic matrix and secondary cement growth. (A) pyritic corrosion/ staining in the form of dendrites that exist mainly in between the micrite (MicMtx) and spar 2 from the Tepee Buttes, (B) an additional example of pyrite corrosion between micrite and spar 2 from the Tepee Buttes, (C) example of corrosion in the Pillar Rock. All photomicrographs were taken at 4x magnification.
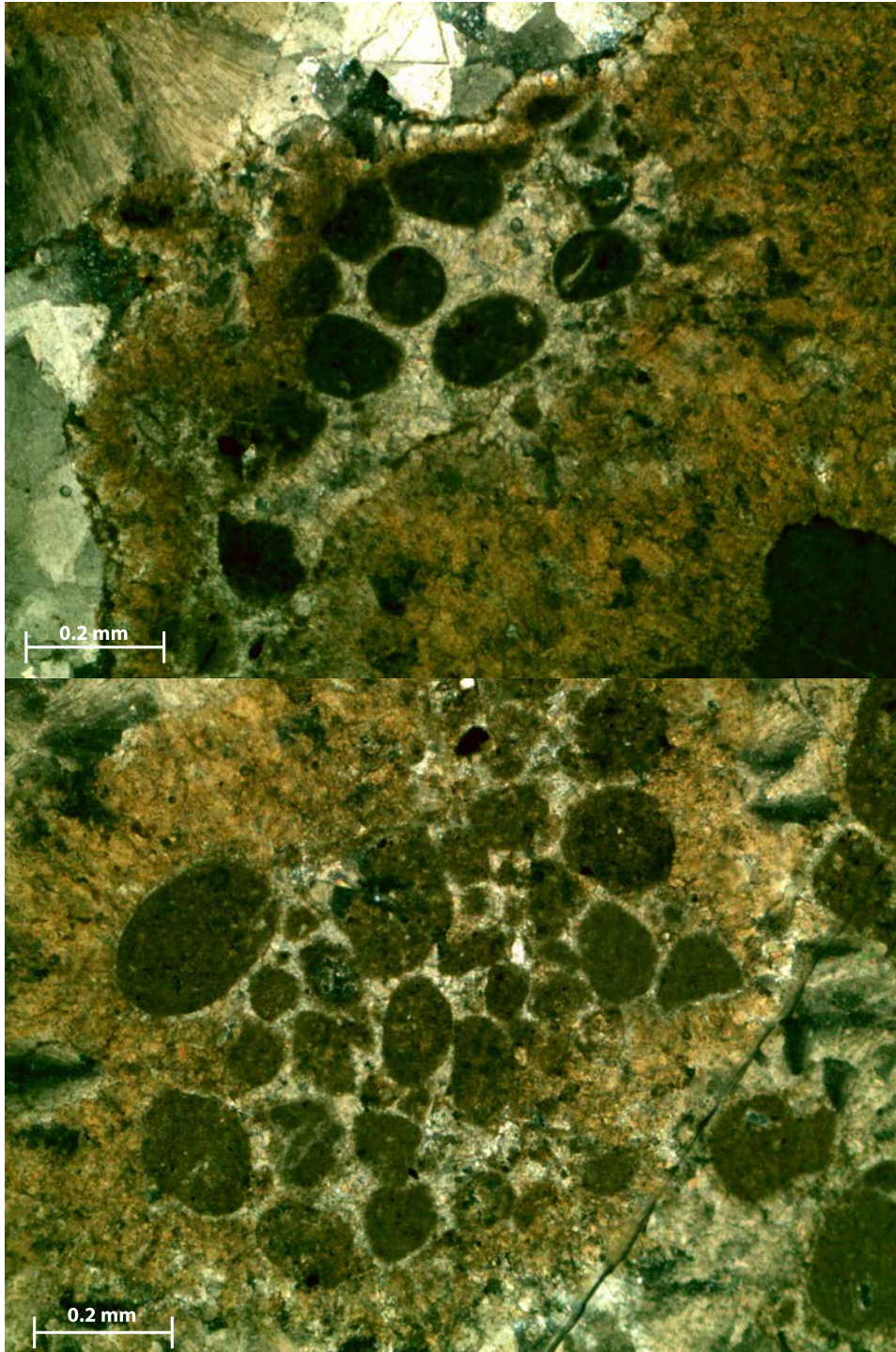
Figure 19 Two examples of peloidal allochems that are fill components of former pore spaces in the Tepee Buttes samples. Both photomicrographs are from Butte 326.5 from the Boone Road outcrop and were taken at 4x magnification.
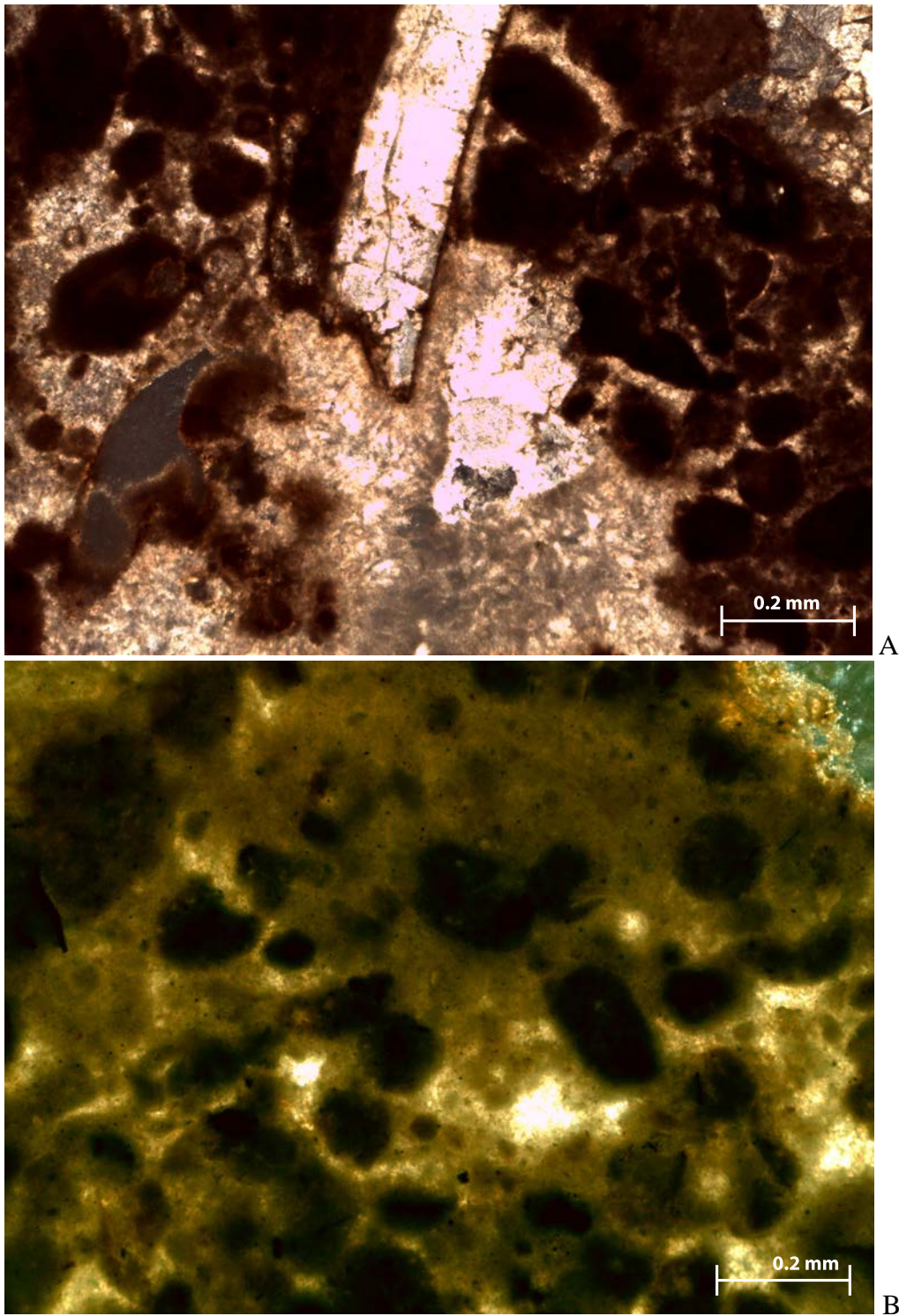
Figure 20 (A) Pelbiosparite allochem/ poorly-sorted peloids filling in void space around bivalve shell fragment. Photomicrograph is from Butte 326.5, (B) Pelmicrite allochem/ well-sorted peloids that are fairly evenly distributed within micritic matrix. Photomicrograph is from Butte 710. Both photomicrographs were taken at 4x magnification.
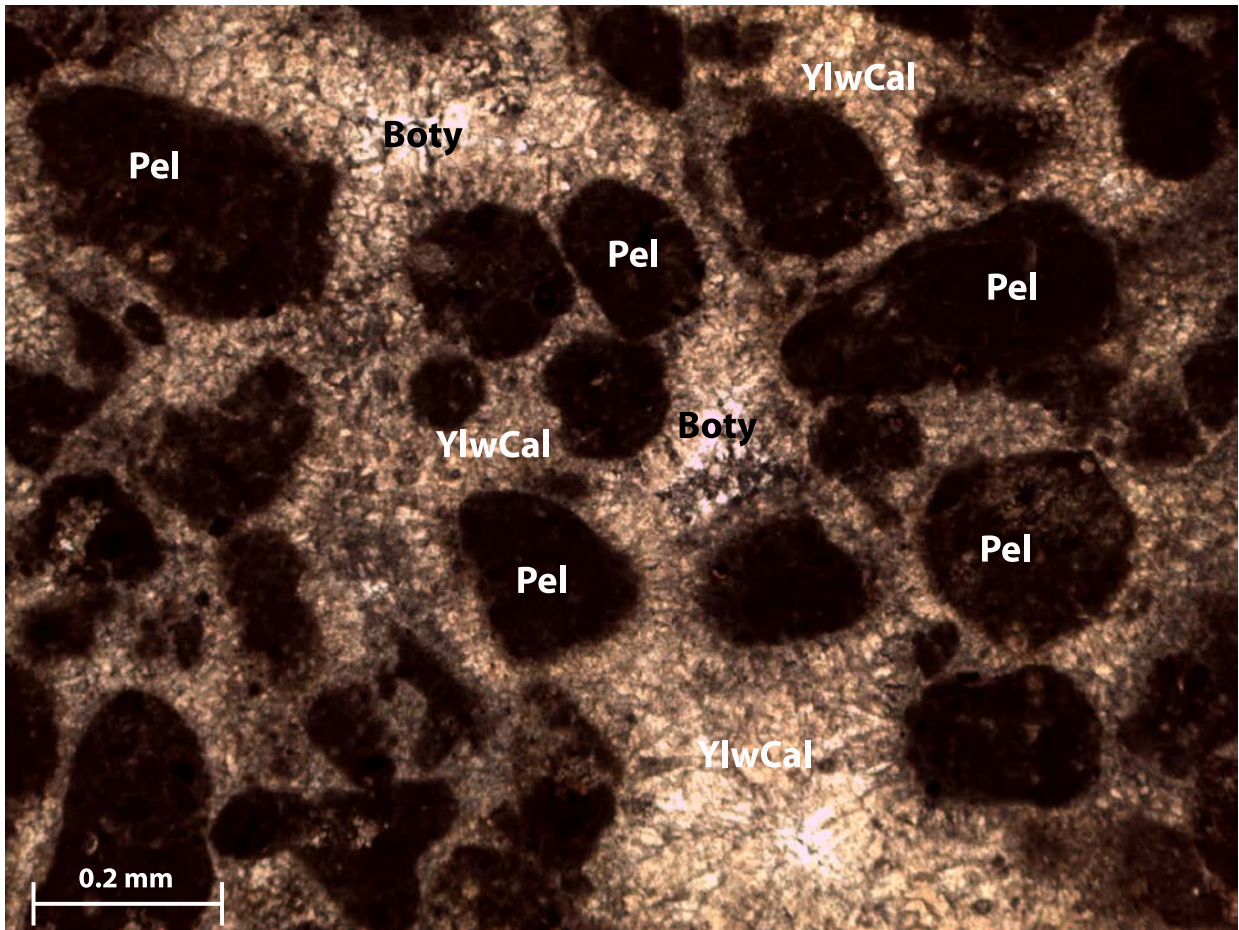
Figure 21 Loose peloids (Pel) with yellow calcite (YlwCal) and botryoid cement (Boty).
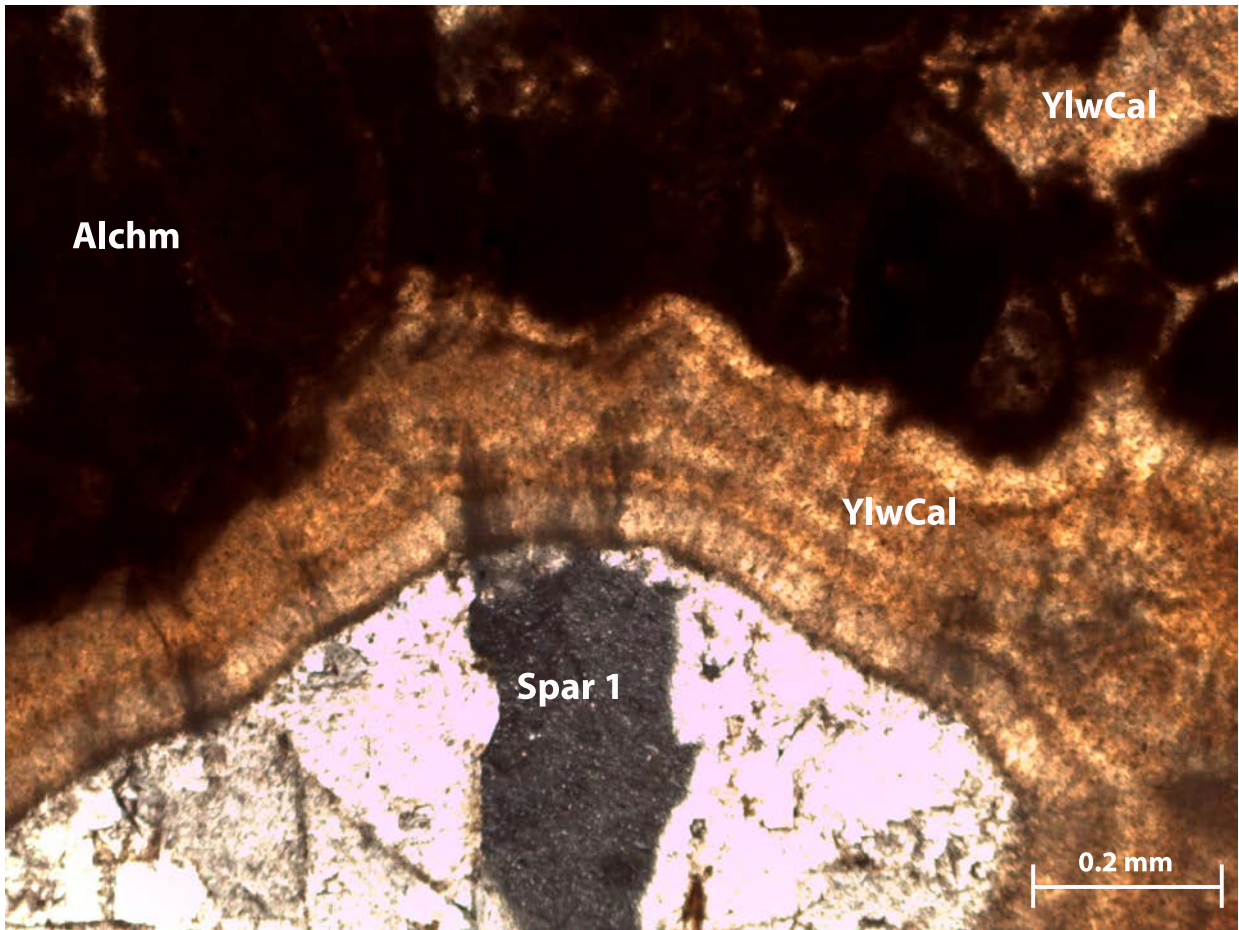
Figure 22 Thick Yellow Calcite noting boundary between spar 1 and peloidal allochems.
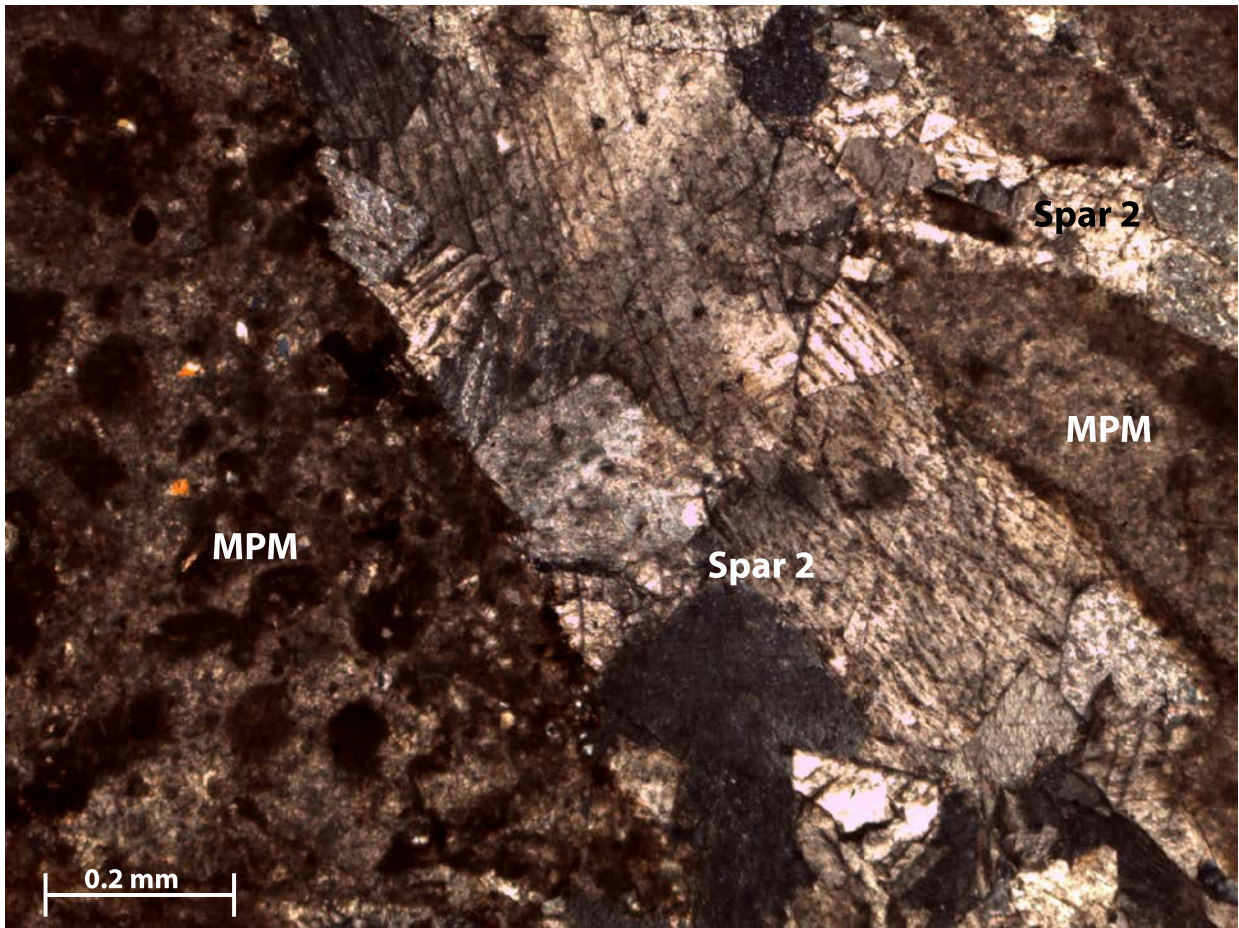
Figure 23 Spar in bivalve shell, extruding into pore space and cross-cutting the micritic peloidal matrix (MPM).
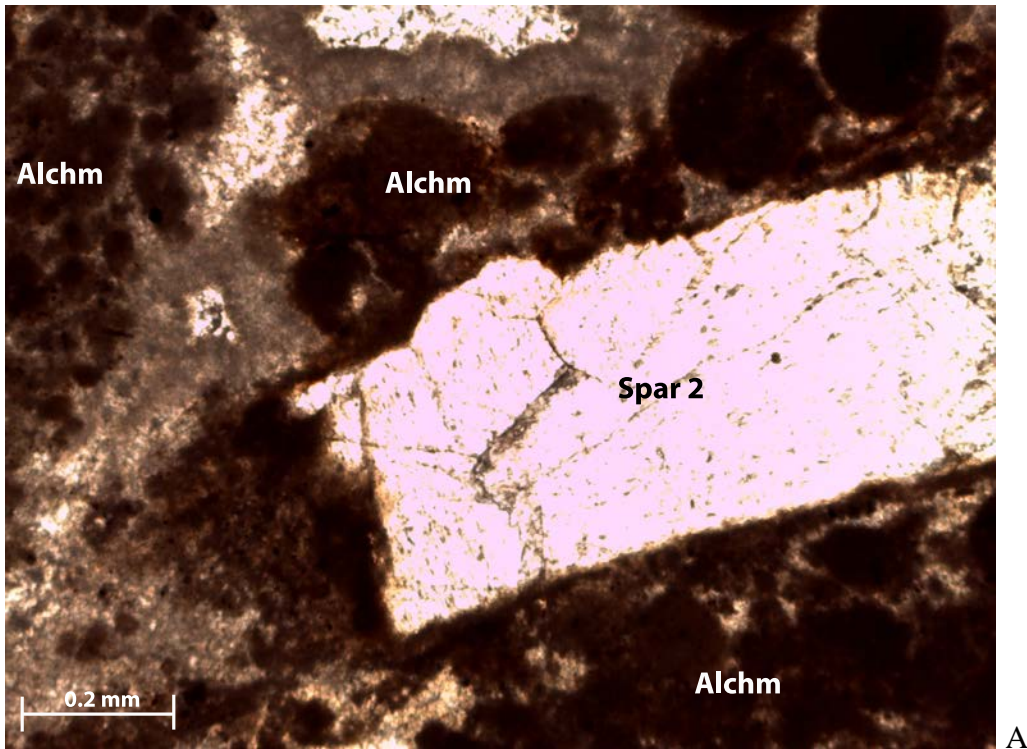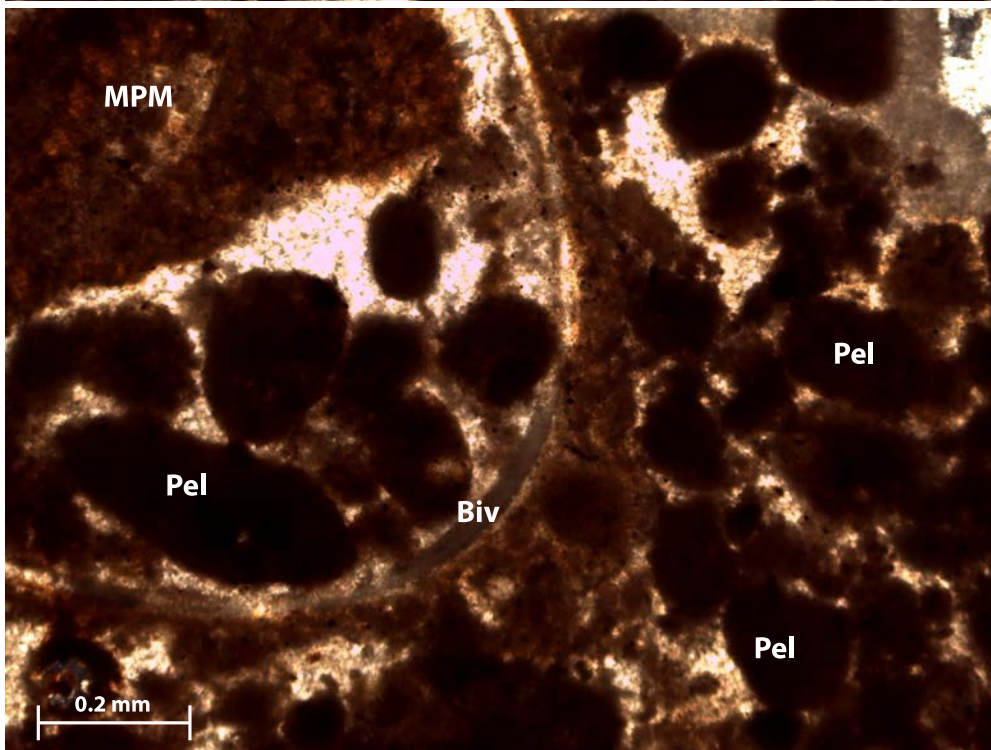
Figure 24 (A) Peloidal allochems cross cut by a bivalve shell (spar 2). (B) Preferential orientation of loose peloids within a bivalve shell fragment.

Figure 25 Thin Section photomicrograph in crossed polarized light of Tepee Buttes (sample 003) showing microbial growth preservation (dark-gray blotches in the matrix).
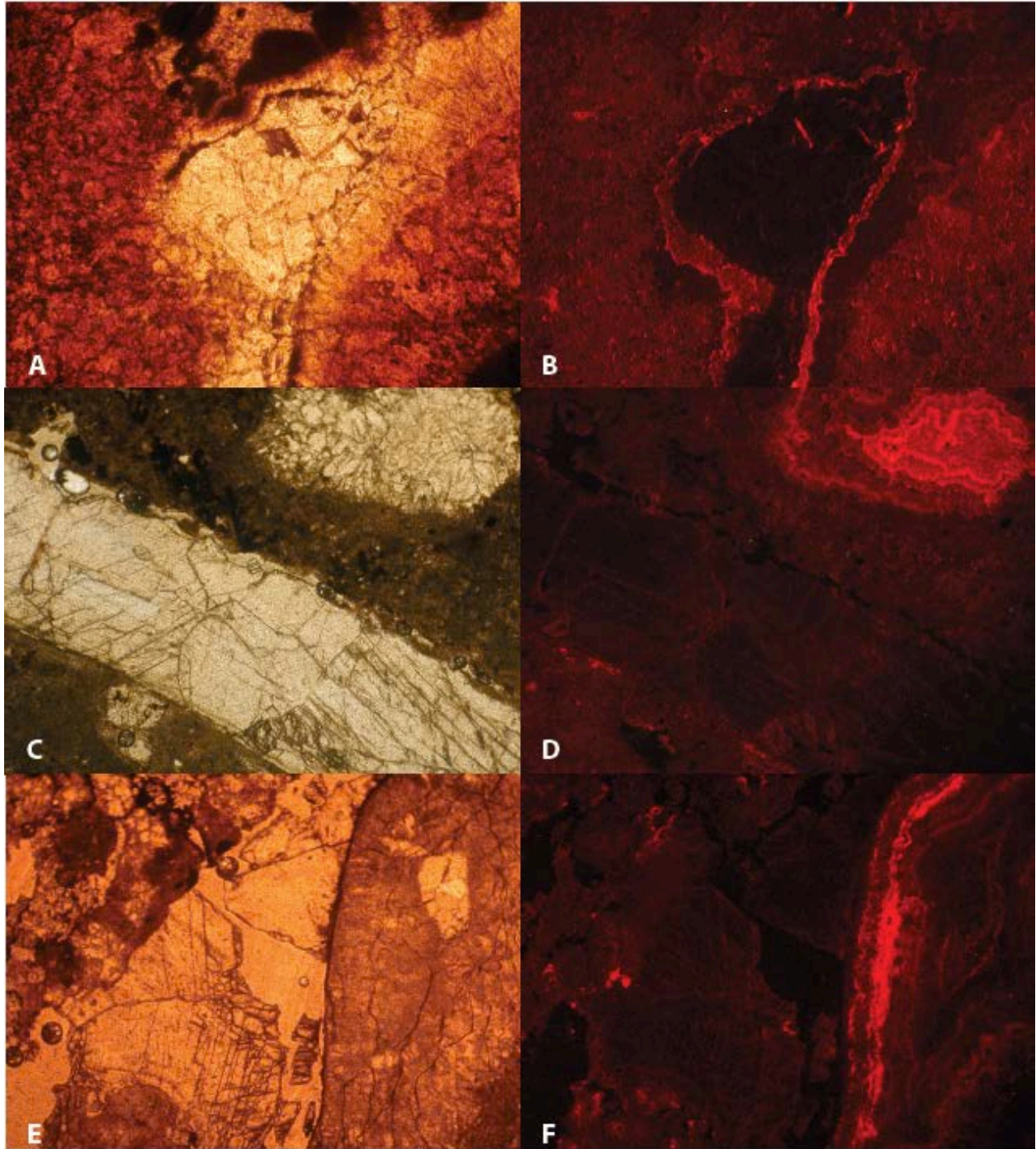
Figure 26 Cathodoluminescence photomicrographs of Tepee Buttes Rocks. Images A, C, and E are non-luminescent images of the corresponding CL images B, D, and F, respectively. Note that (D) shows two stages of sparry calcite exhibiting different reactions to the cathodoluminescence. All photomicrographs are set at 4x magnification.

Sample Area	Sample Names	δ¹³C (‰ VPDB)	δ¹⁸O (‰ VPDB)
OCSG	PR Galveston_03	**-36.6**	**1.9**
	PR Galveston_07	**-40.4**	**2.0**
	PR Galveston_04	**-34.5**	**2.2**
	PR Galveston_05	**-37.9**	**2.2**
	PR Galveston_06	**-38.2**	**2.2**
	PR Galveston_01	**-37.9**	**2.2**
	PR Galveston_02	**-33.6**	**2.2**

Sample Area	Sample Names	Fabric Type	δ¹³C (‰ VPDB)	δ¹⁸O (‰ VPDB)
Tepee Buttes	TPB 007_05	sparry calcite vein	**-22.5**	**-10.0**
	TPB 007_04	sparry calcite vein	**-23.1**	**-10.2**
	TPB 007_02	yellow calcite/peloidal micrite	**-30.4**	**-10.6**
	TPB 007_03	yellow calcite/peloidal micrite	**-31.0**	**-11.0**
	TPB 007_01	yellow calcite/peloidal micrite	**-30.5**	**-12.2**
	TPB 014_04	sparry calcite vug	**-12.5**	**-2.9**
	TPB 014_02	peloidal micrite/allochems	**-37.1**	**-5.9**
	TPB 014_01	peloidal micrite/allochems	**-32.1**	**-9.5**
	TPB 014_03	sparry calcite vein	**-23.9**	**-11.3**

Table 8 (OCSG) Isotopic values showing differences with respect to fabric phases for Gulf of Mexico samples. Red highlighted samples indicate more heavily cemented (botryoid dominated) cement. (Tepee Buttes) Isotopic Values connected with different fabric types for the Pillar Rock samples. Note two phases of calcite cement infilling growth indicated by label as well as large difference in isotopic signature. TPB 007 corresponds to Butte 326.5 and TPB 014 corresponds to Butte 710.
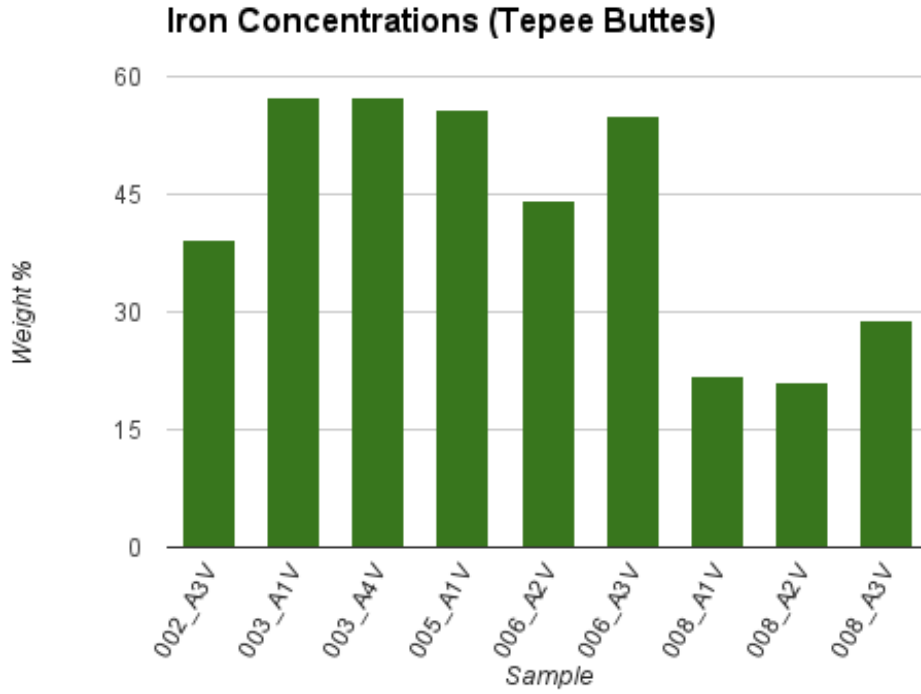
Figure 27 Weight percent iron of Tepee Buttes sample obtained using an SEM. Each bar represents the average iron value of many spot analyses for each sample.
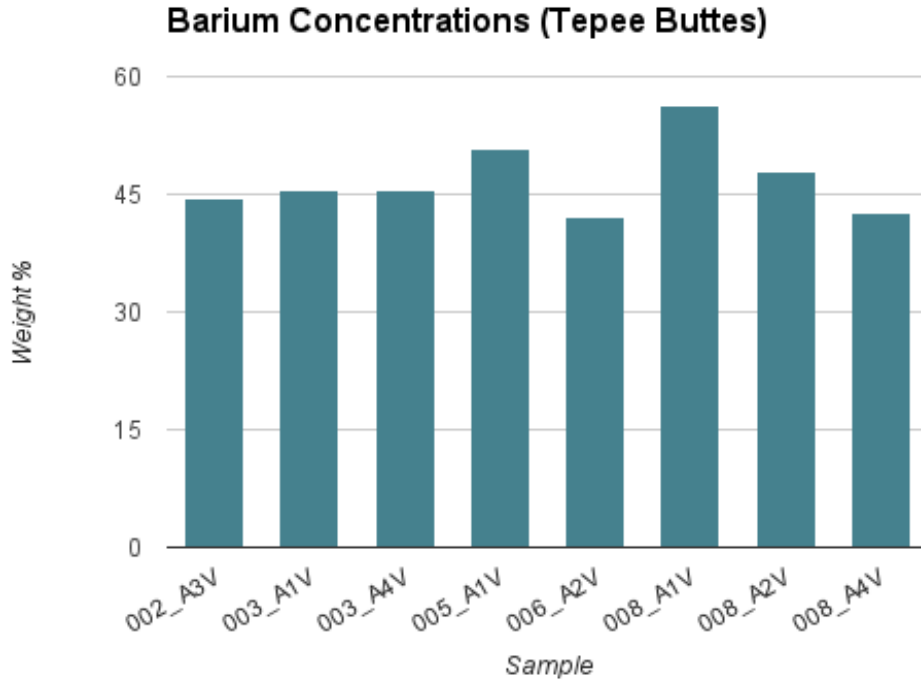
Figure 28 SEM Electron Diffraction Spectroscopy data for several Tepee Buttes samples. Points of interest analyzed showed an average of 40 to 60 weight percent Barium per sample. Each bar represents the average barium value of many spot analyses for each sample.
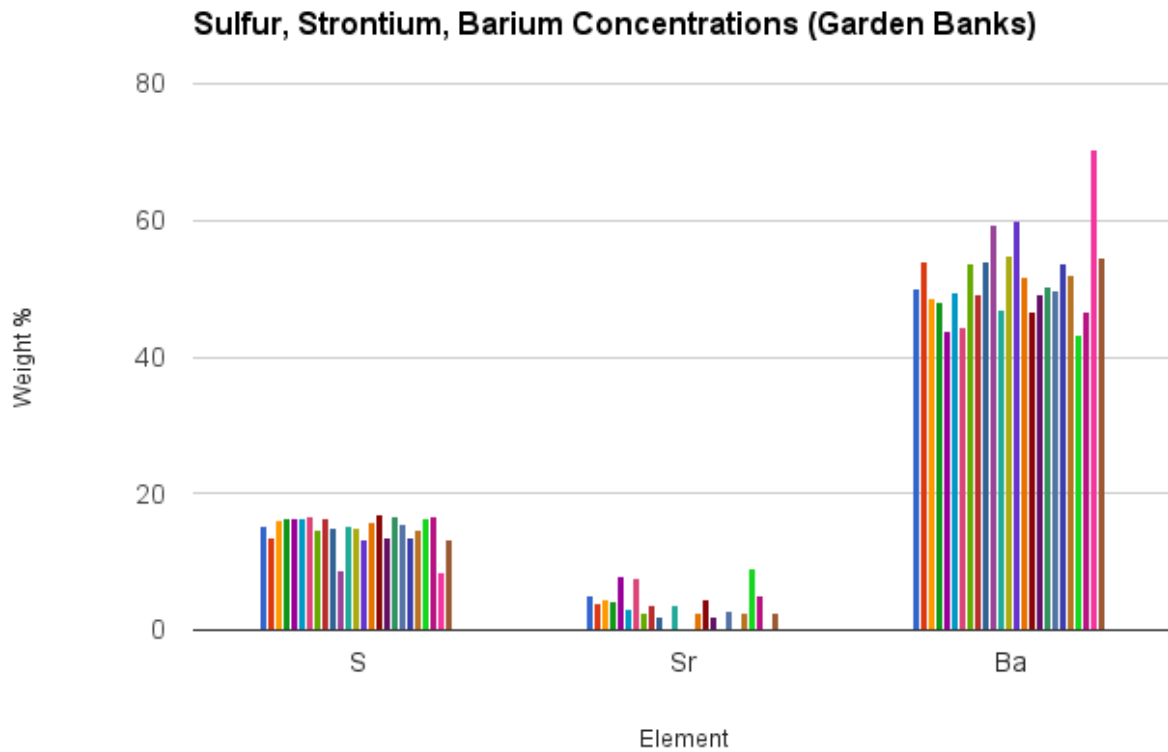
Figure 29 Weight percents of sulfur, strontium, and barium for 25 individual spot analyses from three different thin section samples. Average weight percent from all spots was ~15% sulfur, ~3% strontium, and 51% barium.
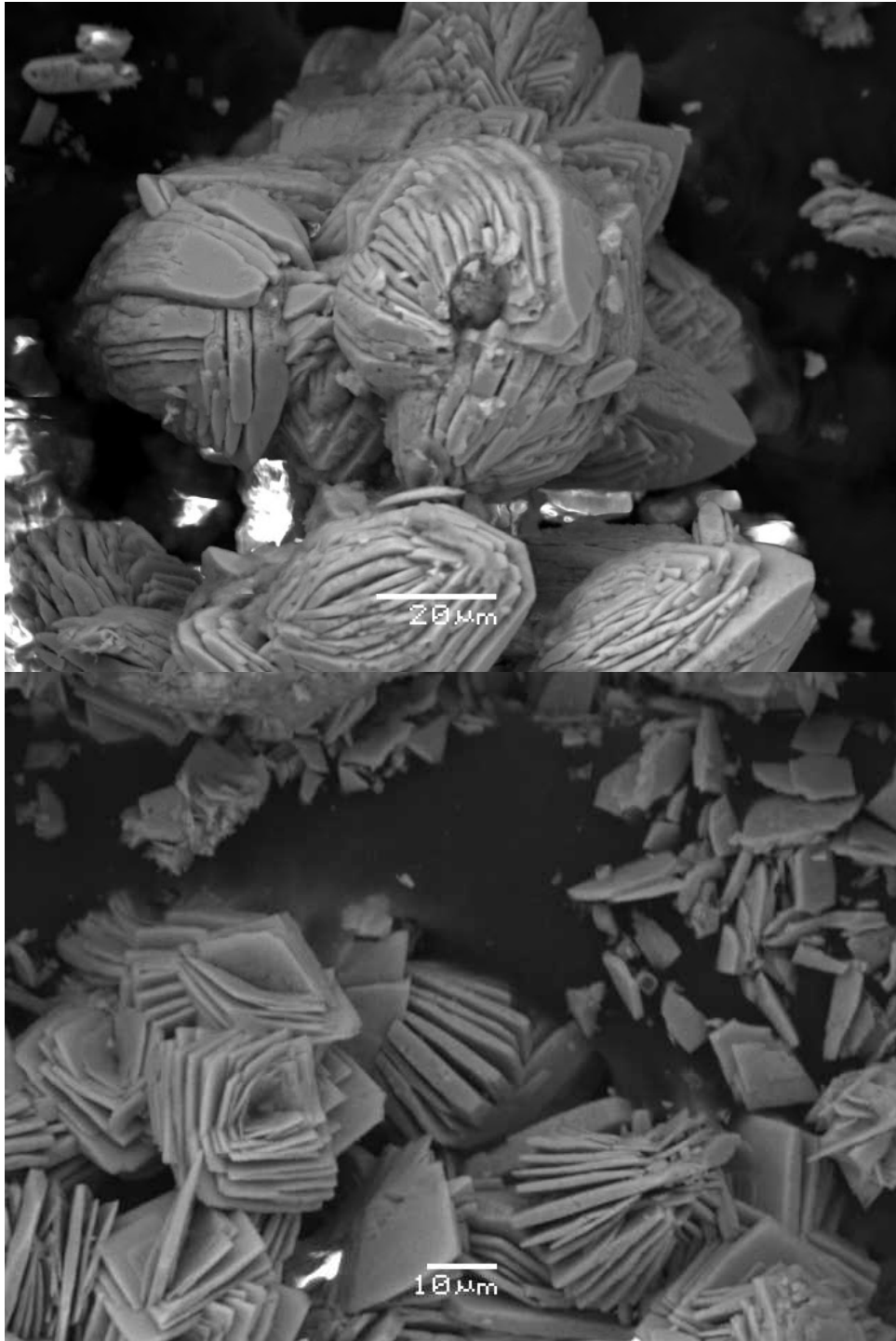
Figure 30 SEM images of characteristic barite crystal rosette structure from the Garden Banks sample (GB425).

mm
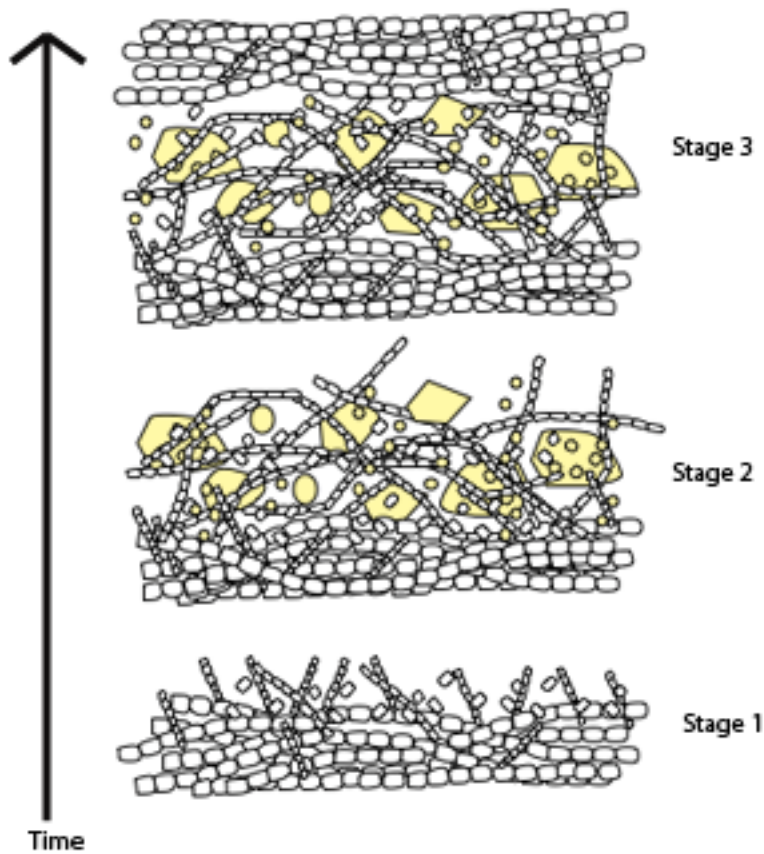
Figure 31 Typical formation sequence of microbial mats with time. Stage 1 depicts the initiation of microbial and bacterial activity. During stage 2, microbial growth occurs and sediment particles are trapped in the EPS created by the microbes. Overtime, microbes lead to the precipitation of carbonate rock with inclusions of sediment particles. In stage 3, they are increasingly covered by more sediment and must continue to growth toward the sediment surface, leaving behind laminated like structures. (Figure adapted from http://www.jpb-imagine.com/Sharjah/3/32histbioter/doc32/1_Hist_Vie_Terre/2121_Stromato.html)
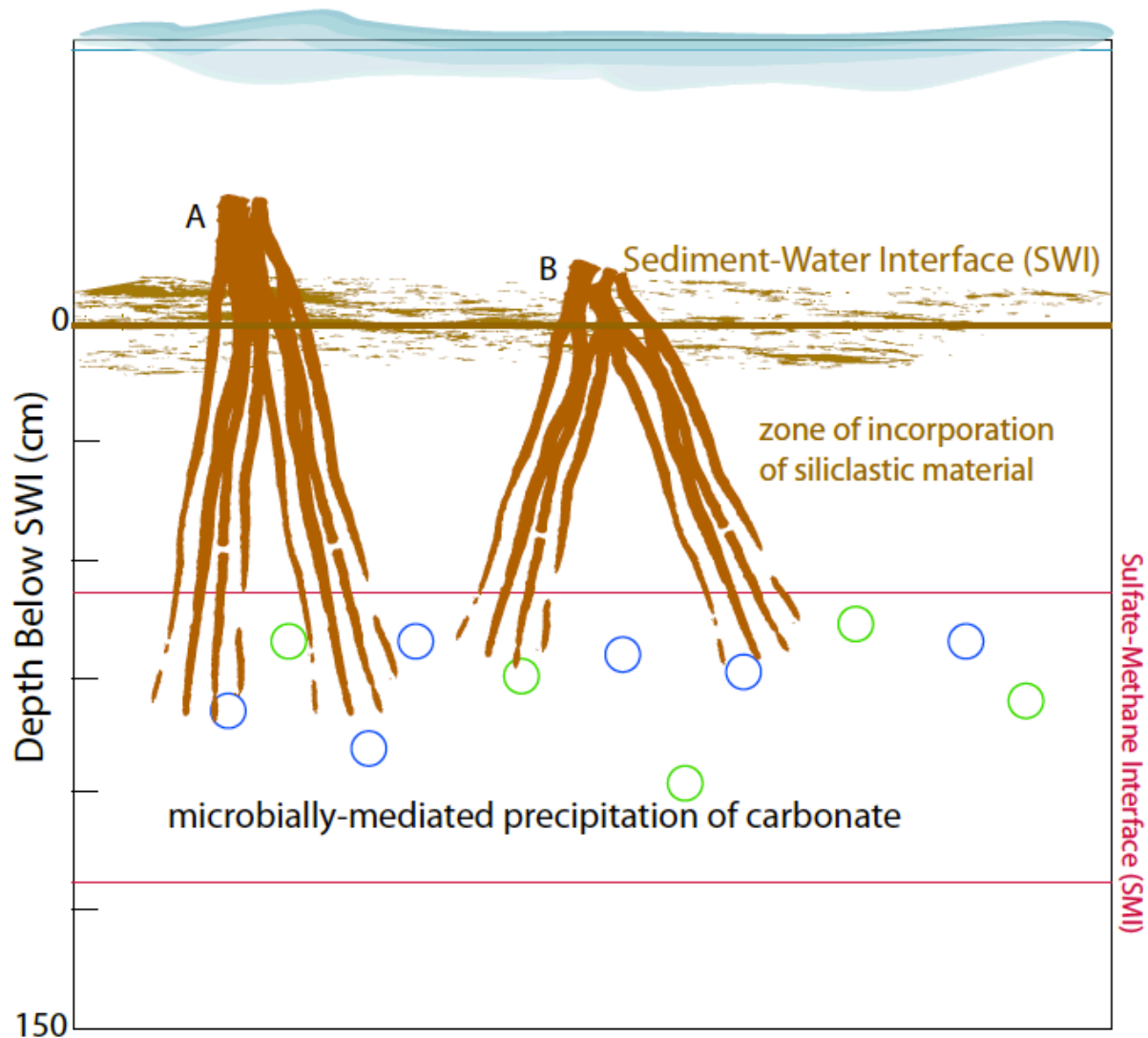
Figure 32 Hypothetical cross-sectional view of the upper 1.5m of seafloor showing proposed initial formation of the Pillar Rock (A) and the Tepee Buttes (B) within the sediment. Both form their fundamental micritic building blocks within the zone of the sulfate-methane interface where they are microbially mediated (blue and green circles indicate presence of at least two types of microbes). Both structures are later exhumed above the sediment-water interface and exposed to seawater that influences the precipitation of cements in pore spaces within the rock.
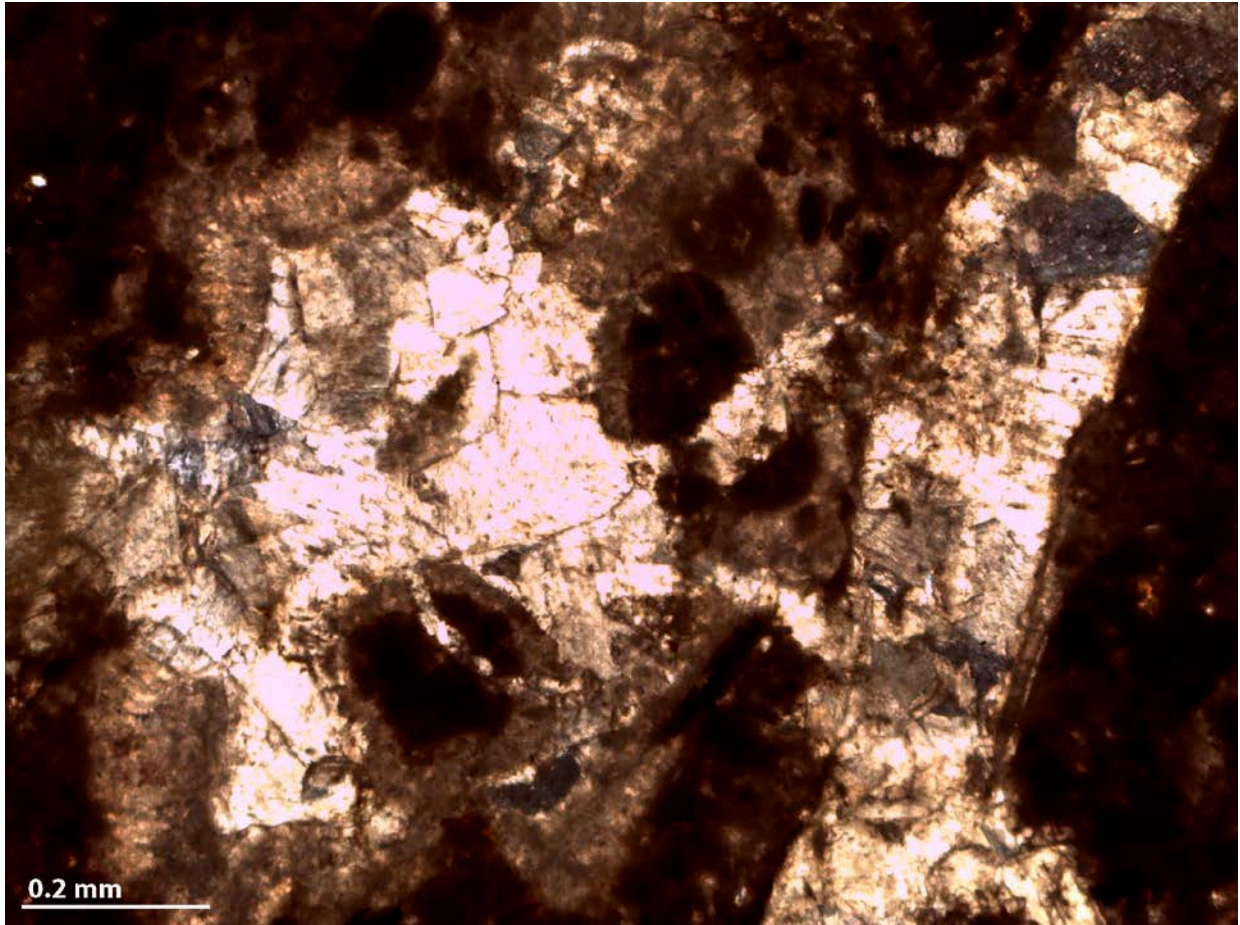
Figure 33 Fractured peloids with a pore space later filled by sparry calcite.